Click Here for Full Article

Midweek increase in U.S. summer rain and storm heights suggests air pollution invigorates rainstorms

Thomas L. Bell,[1] Daniel Rosenfeld,[2] Kyu-Myong Kim,[1,3] Jung-Moon Yoo,[4] Myong-In Lee,[1,3] and Maura Hahnenberger[5]

[1]   Tropical Rainfall Measuring Mission (TRMM) satellite estimates of summertime rainfall over the southeast U.S. are found on average to be significantly higher during the middle of the work week than on weekends, attributable to a midweek intensification of afternoon storms and an increase in area with detectable rain. TRMM radar data show a significant midweek increase in the echo-top heights reached by afternoon storms. Weekly variations in model-reanalysis wind patterns over the region are consistent with changes in convection implied by the satellite data. Weekly variations in rain gauge averages are also consistent with the satellite estimates, though possibly smaller in amplitude. A midweek decrease of rainfall over the nearby Atlantic is also seen. EPA measurements of surface particulate concentrations show a midweek peak over much of the U.S. These observations are consistent with the theory that anthropogenic air pollution suppresses cloud-drop coalescence and early rainout during the growth of thunderstorms over land, allowing more water to be carried above the $0°C$ isotherm, where freezing yields additional latent heat, invigorating the storms and producing large ice hydrometeors. The enhanced convection induces regional convergence, uplifting and an overall increase of rainfall. Compensating downward air motion suppresses convection over the adjacent ocean areas. Pre-TRMM-era data suggest that the weekly cycle only became strong enough to be detectable beginning in the 1980's. Rain-gauge data also suggest that a weekly cycle may have been detectable in the 1940's, but with peak rainfall on Sunday or Monday, possibly explained by the difference in composition of aerosol pollution at that time. This "weekend effect" may thus offer climate researchers an opportunity to study the regional climate-scale impact of aerosols on storm development and monsoon-like circulation.

1.   Introduction

[2]   The effect of pollution on rainfall has been observed to depend both on the type of pollution and the precipitating environment [*Rosenfeld*, 1999, 2000; *Phillips et al.*, 2002; *Jacobson and Kaufman*, 2006]. Pollution aerosols have been documented to suppress precipitation from shallow clouds (cloud heights below about the $−10°C$ isotherm) [*Albrecht*, 1989; *Rosenfeld*, 1999, 2000; *Rosenfeld et al.*, 2002]. When polluted clouds develop to greater heights, however, as often happens in the summertime over land, Rosenfeld suggested [*Williams et al.*, 2002; *Andreae et al.*, 2004] that suppressed rainout enables unprecipitated cloud droplets to reach greater heights where their freezing can release additional latent heat and further invigorate the cloud updrafts. This might in turn delay the onset of precipitation and the development of downdrafts and so prolong the growth of the convective cloud, allowing more water vapor to be ingested and further invigorate the storms [*Rosenfeld*, 2006]. Some recent cloud simulations by *Khain et al.* [2005], *Seifert and Beheng* [2005], *Wang* [2005], *Lynn et al.* [2005], and *Teller and Levin* [2006] support the possibility that in a moist, unstable atmosphere such as prevails during the summer in the southeast (SE) U.S., pollution aerosols can induce clouds to develop stronger

[1]Laboratory for Atmospheres, NASA/Goddard Space Flight Center, Greenbelt, Maryland, USA.
[2]Institute of Earth Sciences, The Hebrew University of Jerusalem, Jerusalem, Israel.
[3]Goddard Earth Sciences and Technology Center, Univ. Maryland Baltimore Cty., Baltimore, Maryland, USA.
[4]Department of Science Education, Ewha Womans University, Seoul, South Korea.
[5]Meteorology Department, University of Utah, Salt Lake City, Utah, USA.

updrafts and downdrafts, grow taller, trigger secondary storm development, and produce more rain. Model simulations of the aerosol-induced invigoration of convective storms do not always lead to increased simulated rainfall, however [e.g., *Wang*, 2005; *van den Heever et al.*, 2006]. These variations in model behavior no doubt depend on a number of factors such as model parameterizations, domain size, and initial and boundary conditions for the simulations that remain to be identified.

[3] Satellite observations also appear to show that cloud area increases and clouds develop to greater heights in more polluted air masses over the Atlantic Ocean [*Koren et al.*, 2005] and over the Amazon basin [*Lin et al.*, 2006]. *Myhre et al.* [2006] show that little of the observed increase in cloud cover and cloud top height can be explained as a simple consequence of changing meteorological conditions.

[4] It is well established [*Simmonds and Keay*, 1997; *Salcedo et al.*, 1999; *Marr and Harley*, 2002; *Beirle et al.*, 2003; *Blanchard and Tanenbaum*, 2003; *Bae et al.*, 2004; *Jin et al.*, 2005] that pollution levels change with the day of the week in many urban areas, generally attributed to changes in vehicular traffic, though variations in power generation may also play a role. We provide examples of the widespread nature of this weekly variation over the U.S. in the next section.

[5] Such variations serve, in effect, as repeated experiments on the consequences of pollution. Weekly variations in temperature, pressure, cloud characteristics, hail and lightning are observed in many areas [*Lawrence*, 1971; *Fujibe*, 1987; *Gordon*, 1994; *Cerveny and Balling*, 1998; *Dessens et al.*, 2001; *Marr and Harley*, 2002; *de F. Forster and Solomon*, 2003; *Mullayarov et al.*, 2005; *Jin et al.*, 2005; *Gong et al.*, 2006; *Bäumer and Vogel*, 2007]. Searches for a weekly cycle in urban precipitation, however, have yielded mixed results [*Cehak*, 1982; *Simmonds and Kaval*, 1986; *Simmonds and Keay*, 1997; *DeLisi et al.*, 2001; *Jin et al.*, 2005; *Gong et al.*, 2006]. Over the Atlantic near the east coast of the U.S., *Cerveny and Balling* [1998] ("CB" hereafter), using rain estimates from the Microwave Sounding Unit (MSU) on TIROS-N satellites for 1979–1995, found a weekly cycle in precipitation with peak rainfall occurring on Saturday and minimum rainfall on Monday. A recent paper by *Bäumer and Vogel* [2007] finds a weekly cycle in a number of meteorological variables measured at 12 stations in Germany. Precipitation averaged over 15 years (all months) seems to peak on Saturday, as does cloud amount, but the daily averages used to find the peaks are somewhat noisy.

[6] Here we examine rainfall statistics from the Tropical Rainfall Measuring Mission (TRMM) satellite [*Kummerow et al.*, 2000] over the southern U.S. and adjacent waters. We supplement the satellite evidence with reanalysis data and rain gauge data (described later). The TRMM satellite has been orbiting the Earth since late 1997. It is unique in that it carries a meteorological radar that can be used to improve the rain estimates made with its passive microwave instrument, the TRMM Microwave Imager (TMI). TRMM's orbital plane is inclined 35° with respect to the Equator. The TMI cannot see poleward of 40°. Because it is in a low-inclination orbit, however, it views areas between roughly 40 S and 40 N at all hours of the day over the course of

46 days, and is able to build up a statistical picture of changes in rainfall statistics both with the time of day and season.

[7] We find a moderately significant midweek increase in daily TMI precipitation estimates over a large portion of the SE U.S. during the summer, and a highly significant midweek increase in afternoon rainfall over the area. TRMM radar measurements of storm heights (echo-top heights) over this area show a substantial midweek increase consistent with the intensification hypothesis outlined above, and reanalysis winds show a midweek increase in low-level wind convergence, mid-level vertical wind velocity, and upper-level wind divergence over the area, consistent with stronger midweek convection. Rain data from gauges are also consistent with the satellite observations, though the amplitude of the midweek increase in daily rain-gauge averages may not be as large as what the TMI data suggest.

[8] Over the nearby waters, the reverse is found: a highly significant weekend peak in TMI-estimated rainfall over the Atlantic and a weaker one over the Gulf of Mexico.

[9] It is important at this point to recall how the TMI is used to obtain rain-rate estimates. Over land the estimates are based mostly on microwave radiance measured by the 85-GHz channel. Since the 85-GHz signal is largely determined by the size and amount of ice aloft, which increases with the intensification of convection in summer storms, this method of estimating rainfall at the surface generally works quite well [*Kummerow et al.*, 2001]. However, the size and amount of ice aloft can increase when more air pollution is added to the clouds while producing the same surface rain intensity [*Rosenfeld and Ulbrich*, 2003; *Khain et al.*, 2005]. It is therefore possible that the weekly cycle in the TRMM rain estimates may be partially due to changes in the ice aloft that are not necessarily accompanied by such large changes in rainfall amounts at the surface. As we shall see, however, the gauge data appear to show a weekly cycle smaller but still comparable in size to the cycle in the TMI data. The dynamical implications of day-of-the-week changes in ice aloft for cloud structure would be important, however, even if surface rainfall were to be unaffected.

[10] These observations open a window to the effects of anthropogenic pollution on regional rainfall at climatological scales. The intensification over land and what appear to be compensating effects over adjacent waters support the suggestion that air pollution suppresses cloud drop coalescence and early rainout, allowing subsequent invigoration of the thunderstorms and outflow aloft. It suggests that summer rainfall on large scales both increases and intensifies as pollution levels rise. The increases in frequency of heavy rainfall events over the U.S. during recent decades found by *Groisman et al.* [2004] may be partly explained by this mechanism.

[11] In the following section we analyze data for particulate aerosols and show that surface aerosol concentrations generally peak in the middle of the week over large areas of the U.S. In Section 3 TRMM (TMI) data are used to look for a weekly cycle in precipitation, and a distinct weekly cycle is found over the SE U.S. and neighboring waters. When rainfall is separated into morning and afternoon amounts, the weekly changes are found to be statistically highly significant. In Section 4 we examine TRMM radar data for echo-top heights and find a dramatic midweek
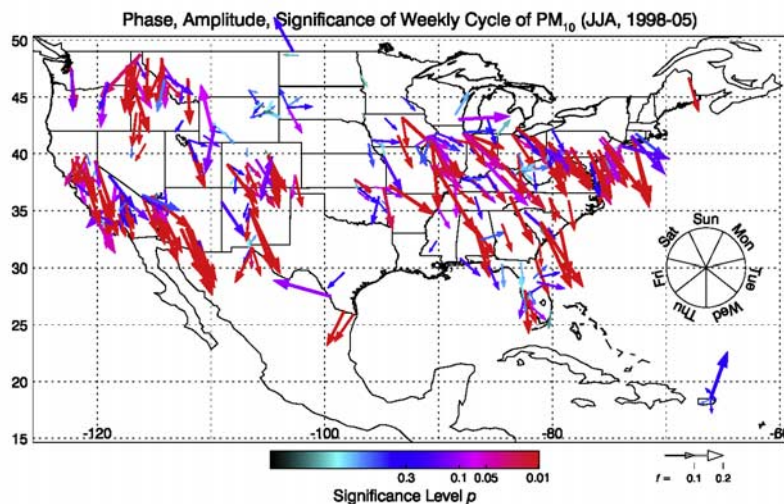
Figure 1. Day of week of maximum of sinusoidal fit to daily PM_{10} measurements at 132 sites in the U.S., and to daily averages of hourly PM_{10} measurements at 254 sites. The lengths of the arrows indicate the amplitude of the weekly cycle as a fraction f of the mean PM_{10} concentration. See length scale at bottom right. Keys to directions are shown in clock format at right. A vector pointing straight up would indicate that the sinusoidal fit to the daily PM_{10} values peaks precisely on Sunday. The colors of the arrows indicate the statistical significance level p of the weekly cycle.

increase in rain frequency and in heights reached by the most intense storms. In Section 5 we find that reanalysis data for atmospheric winds indicate weekly variation in wind patterns over the same areas that is consistent with the weekly cycle in convective activity. We also examine rain gauge data and reanalysis estimates of vertically integrated moisture convergence and compare them with TRMM. In Section 6 we look for signs of a weekly cycle in daily rain gauge data and reanalysis winds prior to the TRMM era. Results are discussed in Section 7, and our conclusions presented in the final section. Two appendices provide additional information concerning the analysis.

2. Weekly Cycle of PM_{10} and $PM_{2.5}$

[12] Pollution varies with the day of the week in many areas of the world. Some examples of observations of a weekly cycle for various types of pollution are provided, for instance, by *Cleveland et al.* [1974], *Simmonds and Keay* [1997], *Cerveny and Balling* [1998], *Salcedo et al.* [1999], *Diem* [2000], *Marr and Harley* [2002], *Bae et al.* [2004], *Harley et al.* [2005], *Jin et al.* [2005], and *Shutters and Balling* [2006]. *Beirle et al.* [2003] and *Beirle et al.* [2004] provide a nice global perspective using satellite observations of the weekly cycle in NO_2 production.

[13] It is informative to see just how widespread the weekly cycle in pollution over the U.S. is by analyzing data for particulate concentrations obtained from the Environmental Protection Agency (EPA) Technology Transfer Network Air Quality System [*USEPA*, 2006]. EPA measurements of concentrations of particulates smaller than 2.5 μm ($PM_{2.5}$) and 10 μm (PM_{10}) have been made for many years at locations around the U.S. at regular time intervals ranging from days to hours. They are generally reported in units of μg m^{-3}. Discussions of $PM_{2.5}$ and PM_{10} measurements may be found in *Wilson* [2002] and *Dye et al.* [2003].

[14] EPA data for years 1998–2005, June–August, were analyzed. The data were current as of 24 August 2006. Where available, daily values of $PM_{2.5}$ and PM_{10} were used. In addition, for those sites where hourly rather than daily values of PM_{10} were available, the hourly values were averaged to daily values, excluding days missing more than 6 hourly values. Days containing negative hourly readings were also discarded, as suggested by *Dye et al.* [2003] in the case of hourly $PM_{2.5}$ data, as were days with concentrations greater than 200 μg m^{-3}. Site data for years with fewer than 69 days (75% of 92 days) were discarded. With these criteria, 212 sites provided 1–8 summers of data for $PM_{2.5}$, while 386 sites provided data for PM_{10}. Some "sites" are quite close to each other physically and are mostly distinguished by the kind of measuring apparatus used. The number of summers of data available at collocated sites may also differ.

[15] Daily data for each of the sites were fit to 7-day sinusoids. Estimates of the statistical significance level p of the sinusoidal amplitudes were obtained following the technique described by *Bell and Reid* [1993]. Some details of the techniques are given in the next section and in Appendix A. The interpretation of a significance level p for a given site is that a spurious weekly-cycle amplitude as large as what is observed, under the hypothesis that no real cycle is present, could occur "by accident" with a probability p determined from an estimate of the level of random variability in weekly excursions. Smaller values of p suggest that the cycle is more likely to be "real".

[16] The maps in Figures 1 and 2 show the results of analyzing the EPA data. Each vector originates from the location of a monitoring site, with its direction indicating the day of the week on which the 7-day sinusoidal fit to the daily averages peaks (see key to directions on right side of maps). The lengths of the vectors show the amplitudes of the weekly cycle fits, expressed as a fraction f of the mean
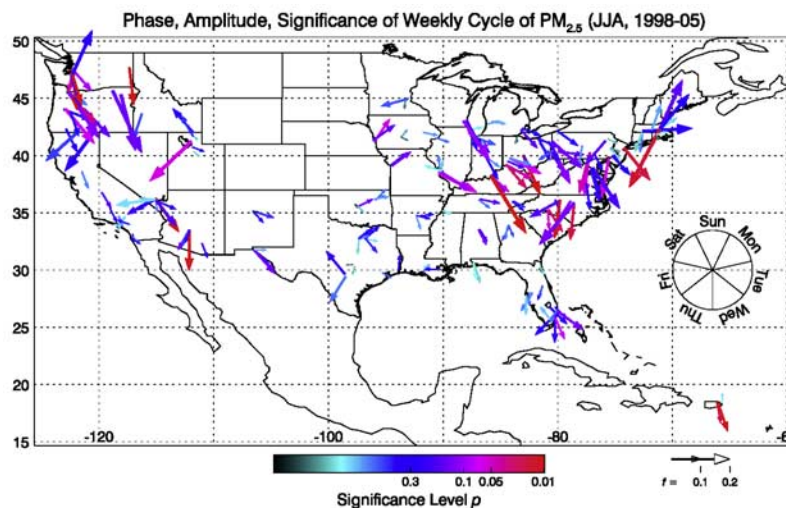
Figure 2. Day of week of maximum of sinusoidal fit to daily $PM_{2.5}$ measurements at 212 sites in the U.S. Lengths and colors of arrows are used to indicate amplitudes and statistical significance levels p of the weekly cycle. See caption to Figure 1 for explanations.

PM concentration, with the key to the lengths shown at the right of the colorbar. A value $f = 0.1$, for example, means that the cycle fit varies by ±10% of the mean PM concentration during the week. The colors of the vectors indicate the statistical significance of the weekly cycle fit, with the colorbar giving the key to the p values for each fit.

[17] It is clear from Figure 1 that there is a widespread tendency for the average concentration of PM_{10} to peak Tue−Thu, although there are almost certainly real differences in the strengths and phases of the cycles depending on location. A midweek peak in $PM_{2.5}$ is also generally evident over much of the U.S. (Figure 2), with notable anomalies in the center of the country. The weekly cycle in $PM_{2.5}$ appears to be weaker than in PM_{10}, perhaps because lighter particles settle out more slowly and are more affected by weather, so that their concentration is less strongly tied to the weekly cycle in emissions. (The lengths of the time series at $PM_{2.5}$ and PM_{10} sites are similar, so the higher level of "noise" in the weekly cycle of $PM_{2.5}$ is not due to differences in the amount of data.) Based on the amplitudes of fits of the data to a sinusoid peaking on Wednesdays, we find that the amplitudes of the weekly cycles of PM_{10} are typically of order ±10% of the mean concentrations, while those of $PM_{2.5}$ are of order ±5% of the mean; but, again, both means and amplitudes surely vary with location.

[18] A number of studies have tried to characterize the weekly changes in particulate concentrations. *Bae et al.* [2004], for example, find that elemental carbon particulate concentrations are about 20% lower on weekends in the neighborhood of East St. Louis, IL. *Marr and Harley* [2002] find that, in the Sacramento/San Joaquin Valleys in California, heavy truck traffic, which mostly uses diesel fuel, is substantially smaller on weekends than weekdays, while daily passenger and light-truck traffic do not vary so much. The results of *Wåhlin et al.* [2001] suggest something similar in the vicinity of Copenhagen, Denmark. *Charron and Harrison* [2005] find that heavy-duty diesel vehicles are responsible for substantial weekly variations in $PM_{2.5}$ and PM_{10} on a major arterial road near London, Great

Britain. *Perry and Owens* [2001] document weekend minima in traffic levels, CO and nitrogen oxide concentrations, and power generation in the Charlotte, North Carolina region.

[19] Observing weekly variations in PM concentrations at the surface does not prove that there is a weekly cycle in cloud-condensation-nuclei (CCN) concentrations at the altitudes where cloud-droplet formation is taking place. The widespread nature of the cycle in surface particulate concentrations does, however, provide some support for the idea that there is a weekly cycle in CCN as well. At the same time, it is worth noting that the weekly cycle in total column aerosol amount may not be nearly as strong as the weekly cycle in near-surface aerosol concentrations as reflected in the measurements of $PM_{2.5}$ and PM_{10} described above. We examined satellite estimates of aerosol optical thickness (AOT) over an area of the southeast U.S. bounded by 32.5 N−40.0 N, 100 W−80 W from the Moderate Resolution Imaging Spectroradiometer (MODIS) aboard both NASA's Terra and Aqua satellites [*Remer et al.*, 2005], using "Collection 4" gridded products MOD08_D3 and MYD08_D3 downloaded using the GES-DISC Interactive Online Visualization ANd aNalysis Infrastructure (Giovanni) as part of the NASA's Goddard Earth Sciences (GES) Data and Information Services Center (DISC). We found that the weekly cycles in both satellites' daytime estimates of AOT were not statistically significant, though sinusoidal fits to both satellite estimates peaked on Wednesday. (The nominal overflight time of Terra is 10:30 AM and that of Aqua is 1:30 PM.) Clearly more research is needed to describe the weekly cycle in CCN concentrations both with respect to their horizontal and vertical distribution and composition.

3. Weekly Cycle in TRMM Rainfall

[20] To look for signs of the influence of weekly variations in human activity on precipitation, averages for each day of the week based on 8 years (1998−2005) of data for
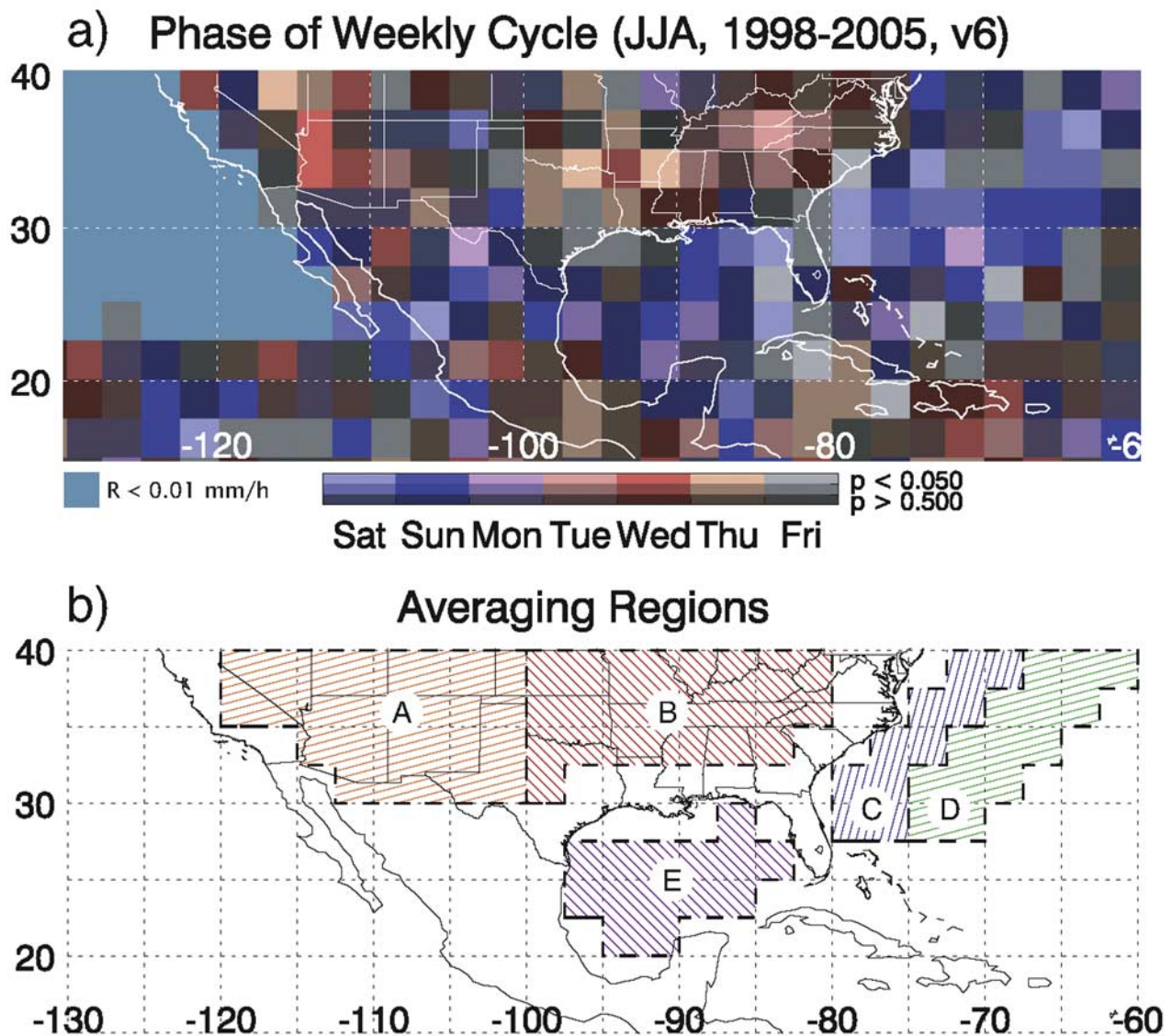
Figure 3. (a) Phases of weekly cycle based on 7-day sinusoidal fits (Equation 1) to daily averages of TRMM TMI rain estimates for 8 summers, for each 2.5° grid box. Colors for each grid box indicate day of the week for which fit is a maximum. Grayness of colors is based on the significance level p for the amplitude, with colors along top of color bar indicating significance level $p < 0.05$. Areas with rain rates less than 0.01 mm h^{-1} are masked. (b) Five averaging areas A–E chosen to improve the signal-to-noise ratio of the weekly cycle.

summertime (June–August) rain rates, estimated using version 6 of the TMI retrieval algorithm [*Kummerow et al.*, 2001; *Olson et al.*, 2006], were obtained for each 2.5° × 2.5° grid box viewed by TRMM in the vicinity of the continental U.S. (Some results for 2006 will be discussed later.)

[21]   The daily averages $r(t)$ for each grid box were fit to a sinusoidal form

$$r(t) = r_0 + r_7 \cos[\omega_7(t - \phi_7)] \qquad (1)$$

with $\omega_7 = 2\pi/(7 \text{ days})$, t the time measured in days, r_0 the average rain rate, r_7 the amplitude of the weekly cycle, and ϕ_7 the day of the week when the sinusoidal fit peaks. The statistical significance of the amplitude r_7 under the hypothesis that there is no weekly cycle ($r_7 = 0$) was obtained using a technique described in Appendix A. Figure 3a shows a map of the phase ϕ_7 obtained using this fitting procedure. The strongest colors (topmost in color bar) indicate significance levels of r_7 with $p = 0.05$ or better (which it may be helpful to think of as equivalent to amplitudes larger than "2 sigma" for normally distributed errors). Although there is considerable variability in the phase (much of which might be explained by sampling error due to the length of the data set), it appears that there is a tendency for average rain rates to peak during the middle of the week (Tue–Thu, predominantly reddish hues) over the continental U.S., and to peak Sat–Mon over the nearby

Atlantic (predominantly bluish hues) and perhaps the Gulf of Mexico. There also appears to be a tendency for the weekly cycle to weaken near the coasts, in the sense that significance levels tend to be low there, or for the peaks to shift to Friday. Results of studies of data from coastal cities mentioned earlier looking for a weekly cycle in precipitation may have been inconclusive for this reason.

[22] Even with 8 years of data, the statistical uncertainty in the weekly cycle in many of the grid boxes is large. We therefore try to increase the signal-to-noise ratio by averaging over larger areas, guided by our physical understanding of where and how the weekly cycle in pollution is likely to affect precipitation. Summer precipitation over the U.S. differs markedly in the eastern and western halves, due in part to the effects of the moisture brought to the eastern half from the Gulf of Mexico by prevailing winds [see *Jin et al.*, 2005, for example] and in part to the differences in topography. We have therefore calculated average rain rates for the five averaging areas A–E shown in Figure 3b. Grid boxes containing substantial amounts of coastline are excluded, partly based on an apparent reversal of the phase at the coasts and partly based on concerns about the change in the TMI retrieval algorithm that occurs at the coast [e.g., *Kummerow et al.*, 2001]. Area C is identical to the region examined by CB except for two of the 2.5° grid boxes included in their average (spanning 40–42.5 N and 70–65 W) too far north to be seen by TRMM.

[23] Figure 4a shows the average rain rates for each day of the week for areas A-C. Averages are obtained by summing rain-rate estimates for all TMI footprints falling within the area during the averaging period, and dividing by the number of footprints contributing to the sum. (One-sigma error bars for Area-B averages are estimated using the resampling technique described in Appendix A.) The SE-U.S. (area-B) average daily rain rates for Tue–Thu are higher than for Sat–Mon, with a maximum on Tue. The SW U.S. (area A) may have a tendency to have higher midweek rain rates, but the signal is very weak. In contrast, the coastal Atlantic (area C) shows strongest rain rates Sat–Mon and lower rain rates Tue–Thu—almost exactly opposite to what is happening over land. The behavior over area C is similar to what CB found, but their results were based on a different sensor for an earlier time period (1979–1995), and they averaged data over all seasons whereas our averages include only summers. [A fit of Equation (1) to 7 complete years of TMI data (1/98–12/04) for area C peaks on Sunday but has little statistical significance ($p = 0.75$). Our data set thus does not show a statistically significant all-season weekly cycle analogous to what CB found, possibly because it is shorter in length than theirs.]

[24] Figure 5a shows the average rain rates for areas C–E. Statistics for area C have been repeated there to aid comparisons. Both the Atlantic region D (east of region C) and the Gulf of Mexico (area E) seem to show weekend maxima similar to that of C, but weaker.

3.1. Weekly Cycle in Rainy Area and Intensity

[25] The weekly changes in TMI estimates of daily rain rate are due in part to changes in the average fraction of the area covered by rain and in part to changes in the intensity of rain where it is raining. This can be seen in Figures 4b and 4c and Figures 5b and 5c. The average fraction of area

with rain is represented by the daily average fraction of TMI footprints (nominally of order 10 km in diameter) with detectable rain in them for each area, while the average intensity of rain is represented by the ratio of the mean rain rate (Figures 4a and 5a) to the mean fraction-with-rain (Figures 4b and 5b), equivalent to the rain rate averaged over rainy areas only. Linear regression of changes in average rain rate for each day against changes in rainy area and changes in intensity suggests that increases in average rain rate are about 1/3 due to increases in areal coverage by rain and 2/3 to rain intensity. Data for TRMM Precipitation Radar (PR) storm heights that will be discussed in Section 4 also indicate both a midweek increase in storm intensity, as inferred from increased storm heights, and increased areal coverage by rain.

3.2. Statistical Significance of Cycles

[26] The question immediately arises whether these cycles are artifacts of the observational characteristics of TRMM, or accidents arising from the natural variability of precipitation. Evidence that the sampling pattern of TRMM is unlikely to have generated spurious weekly cycles of the magnitude seen here is described in Appendix B. The possibility that the weekly oscillations seen in Figures 4 and 5 are simply residues of random rain events with no favored days of the week is evaluated using a resampling (bootstrap) technique that attempts to take into account the multi-day time correlations of rain and the special sampling pattern of the TRMM satellite. It is described in Appendix A. Figure 6 displays the resampling results for the 5 areas as a "clock plot." The phases ϕ_7 of the fits are indicated by angular position, whose meaning is given by the labeling along the clock perimeter. The statistical significance p of each cycle, estimated using resampling, is indicated by distance from origin, and is proportional to $(-\ln p)^{1/2}$. [As explained in Appendix A, Equation (A2), $(-\ln p)^{1/2} \approx r_7/\sigma_7$, where σ_7 is the estimated "noise" level for the amplitude r_7 of the fit, and so $(-\ln p)^{1/2}$ can be thought of as the "signal-to-noise" ratio of the weekly-cycle amplitude.] Circles with radii corresponding to various values of p are drawn in Figure 6 to define the radial scale.

[27] The weekly cycle of the average over the SE U.S. (area B) is significant at the $p = 0.10$ level. (Parameter values of fits for each area are given in Table 1.) The coastal Atlantic (area C) cycle is significant at the $p = 0.035$ level. The other two areas over water, D and E, have weekly amplitudes that are above "1-sigma" in size. A weekly cycle over the SW U.S. (area A), if present, is not strong enough to be detected with any confidence. In fact, a weakened response over the SW U.S. (area A) is consistent with simulations by *Khain et al.* [2005], which show that invigoration of convection by pollution is diminished in drier conditions, and may even reverse.

[28] [It may be helpful to the reader to be reminded that plots like Figure 6 can serve two purposes: The length of a vector gives the significance level p of the amplitude r_7, indicated by the circles labeled by various values of p, and serves to test the hypothesis $r_7 = 0$. Once one has accepted the hypothesis that there is a weekly cycle ($r_7 \neq 0$) and one wants confidence limits for r_7, ϕ_7, the same plot can provide this if one draws circles centered on the end of the vector with radii equal to those of the circles labeled by p. Thus the
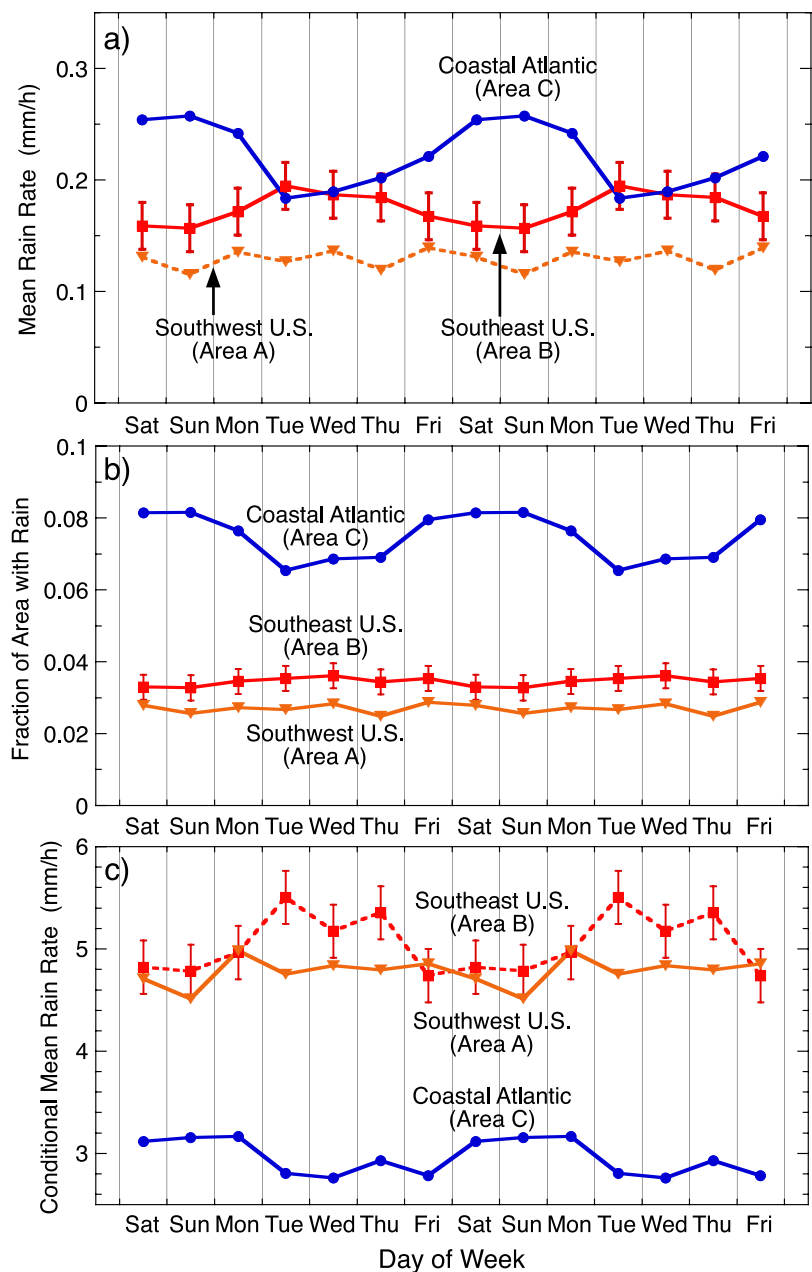
Figure 4. Daily statistics (JJA, 1998–2005) of TMI data for each day of the week for areas A–C delineated in Figure 3b. Area-B error bars are 1-sigma confidence limits determined using bootstrap method. (a) Average rain rate. (b) Fraction of TMI footprints with rain. (c) Ratio of results in panels a and b, indicating intensity of rain where it rains (i.e., conditional on $R > 0$); note vertical scale in panel c.

three circles in Figure 6 can be used to provide the 70%, 90%, and 97% confidence-limit circles for the 5 vectors. It should be remembered that each vector r_7 is plotted scaled by its own "noise" estimate σ_7 (see Appendix A), and so quantitative comparison of two amplitudes r_7 requires replotting of the data with a uniform scale. Additional discussion may be found, for example, by *Collier and Bowman*, 2004].

3.3. Morning Versus Afternoon Statistics

[29] The significance level of the SE-U.S. weekly cycle does not quite reach the "canonical" $p = 0.05$ level. We note, however, that the explanation for the intensification of storms by pollution proposed here would suggest that the intensification should be greatest when atmospheric instability is greatest, since moist parcels of air are carried highest in such an environment. This suggests that the intensification should be greatest for afternoon rainfall, and this is indeed what is seen.

[30] Figure 7 shows the average rain rate for each day of the week for morning rain (0000–1200 LT) and afternoon rain (1200–2400 LT) over area B. Local time (LT) is
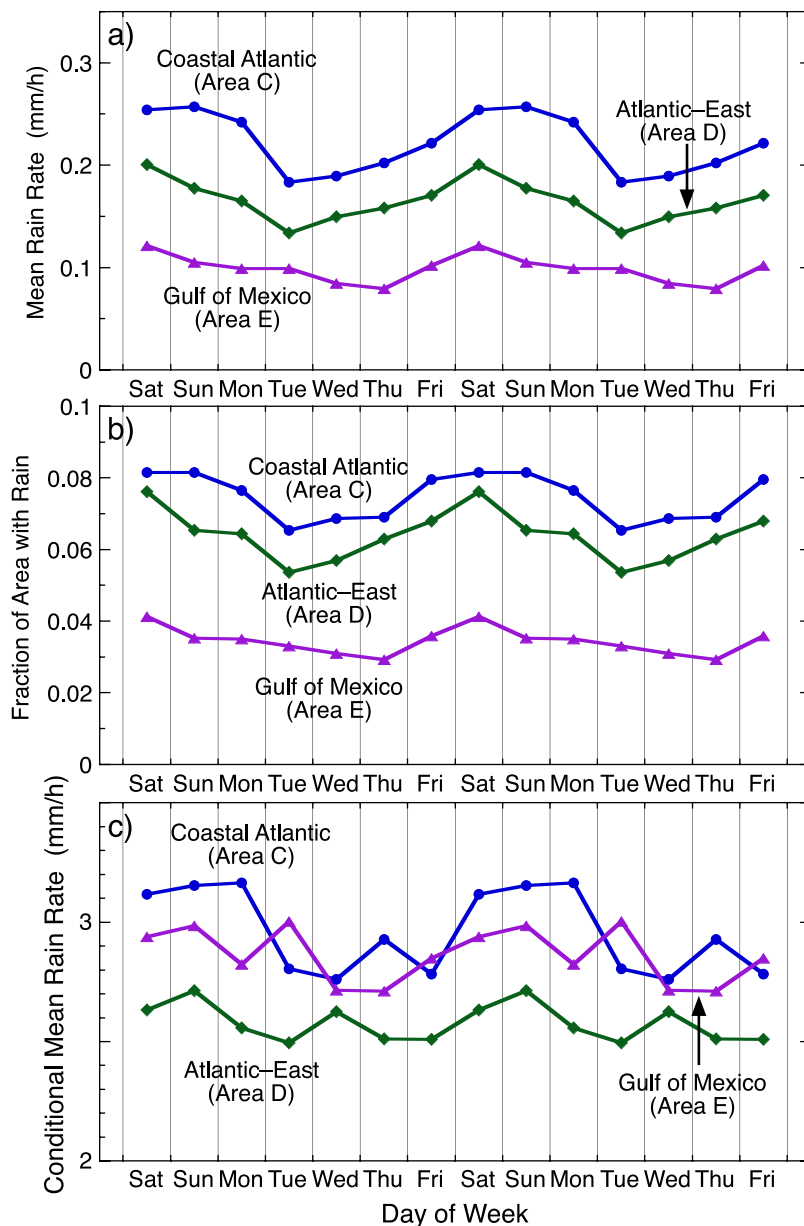
Figure 5. Rain statistics as in Figure 4 for areas C–E in Figure 3b. Statistics for area C in Figure 4 repeated here to aid comparisons. Note vertical scale change in panel c.

computed from the longitude λ $(-180° \leq \lambda < 180°)$ of the centroid of each area as

$$LT = UT + \lambda/(15°/\text{hour}), \qquad (2)$$

where UT is Universal Time. The weekly cycle of afternoon rain is quite strong. It peaks on Tuesdays, and has a very high significance level $p = 0.0012$ when estimated using resampling. The afternoon weekly amplitude is about twice as large as the morning amplitude, which has a significance level $p = 0.045$ and peaks on Saturdays. The impact of the afternoon cycle on daily totals thus seems to be somewhat mitigated by compensating changes in morning rainfall, so that the weekly cycle for daily total rainfall is weaker than for the separate morning/afternoon components. Ways in which precipitation during one part of the day can influence precipitation at other times, thereby affecting the overall diurnal cycle, are discussed by *Betts and Jakob* [2002].

[31] Although not shown here, the relative contributions to the weekly change in afternoon rainfall from changes in rainy area and intensity are rather different from what was inferred from the 24-h totals in Section 3.1: we find about 75% of the weekly peak in rain rates is due to increase in rainy area and 25% to increase in rain intensity. Note, however, that over land the TMI estimates of peak intensities may be underestimated due to saturation of the 85-GHz channel due to the large amount of ice aloft.

[32] The afternoon cycle is so strong that, when individual summers of data are fit to sinusoids, 5 of the 8 summers (1998–2005) peak on Wed, and the remaining 3 on Mon–Tue, as shown in Figure 8a. The sinusoidal fit to TMI data for year 2006, however, peaks on Saturday, with a signif-
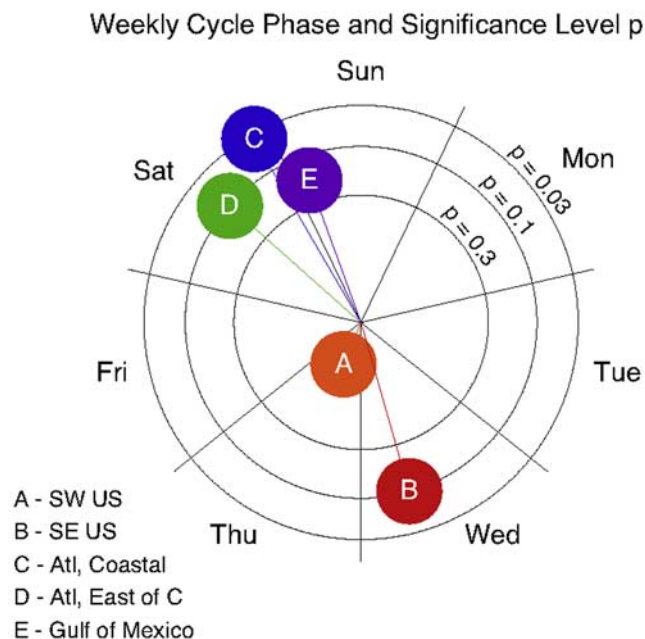
Weekly Cycle Phase and Significance Level p

Figure 6. Phase and significance level of weekly cycles of daily mean rain rate for the 5 areas in Figure 3b. Angular position is determined by day of week with maximum rain rate, based on sinusoidal fits to plots in Figures 4a and 5a. A vector pointing straight up would indicate the maximum occurs on Sunday noon. Radial distance is determined by significance level p of weekly cycle and is proportional to $(-\ln p)^{1/2}$ ("signal-to-noise ratio").

icance level $p = 0.08$ estimated using resampling. In examining the weekly cycles of afternoon TMI data for single summers, however, we should remember that because the TRMM satellite views the U.S. during afternoon hours for about 3 weeks and then spends another 3 weeks observing during morning hours, only about $6-7$ weeks of afternoon data are collected each summer. The estimates for individual years shown in Figure 8a are therefore not based on many weeks of data. To see statistical evidence of a weekly cycle, nature must provide us with a set of trials that are evenly distributed over the days of the week, with similar conditions for storm development but varying pollution levels. If favorable conditions for rain occur at best a few times per week, a single summer of afternoon TMI observations is quite likely to fail to provide us with a set of "experiments" distributed evenly enough for a convincing weekly cycle to be visible in the data.

[33] To get a better feeling for the stability of the yearly estimates in Figure 8a, data from the TRMM Multi-satellite Precipitation Analysis (TMPA) product were analyzed. This TRMM product, 3B42 in the standard TRMM product list, incorporates both data from various satellites carrying microwave instruments, including TRMM, and rain estimates using geosynchronous infrared (IR) data, tuned to match the microwave estimates. The estimates are adjusted where possible to agree with monthly rain-gauge totals. The product provides gridded rain fields every 3 h, and is described by *Huffman et al.* [2007]. Over land, the accuracy of the other microwave rain estimates is likely to be roughly

comparable to that of TMI estimates. The accuracy of the IR estimates is the most problematic, but, on a global basis, the fraction of the data set for which IR estimates are the only information declines from about 55% in 1998 to 20% in 2004 [G. Huffman, 2007, private communication]. Because the TMPA product includes passive microwave data from roughly 4 satellites in addition to TRMM in 2000, increasing to ~6 satellites in 2003–2005 [*Huffman et al.*, 2007], the sample size contributed by microwave estimates in the TMPA product is roughly 4 times as large as from TRMM alone, and, aside from the overall "calibration" of the product, the TRMM contribution to the TMPA sample averages is not particularly large. Although this data set brings along with it a set of remote-sensing and algorithmic issues that are not easy to quantify, we believe it provides a quasi-independent satellite perspective that may be helpful. We have therefore examined the 3-hourly TMPA rain estimates averaged over a rectangular area that is close to that of area B, covering $32.5-40.0$ N, $100-80$ W. The data were acquired using the Giovanni interface mentioned in Section 2. Weekly-cycle fits to each summer of data for the available years 1998–2006 were obtained. The results are plotted in Figure 8b. The estimates for the two most anomalous years 2005 and 2006 have moved closer to those for the earlier years and are weaker in strength. Such changes in the strength of the weekly cycle from year to year are consistent with variations we shall discuss later for data from rain gauges, and suggest that the weekly-cycle signal waxes and wanes in strength from summer to summer.

[34] (This is the only section in which data for 2006 are discussed and the TMPA product is used.)

3.4. Weekly and Diurnal Cycles in TMI Averages

[35] A more detailed picture of the day-night differences in the weekly cycle can be seen in Figure 9, which shows how the weekly cycle of TMI-estimated rain in areas B and C varies with the hour of the day. Note how the cycle over land (area B) is mirrored over the nearby ocean (area C). The afternoon maximum over land on Tuesday is paired with a minimum over the ocean with a delay of ~2 hours. Note also how much weaker the diurnal cycle is on Saturdays than on Tuesdays over area B.

4. TRMM Radar Storm Heights

[36] The mechanism for the midweek intensification of storms proposed here suggests that more storms should reach higher altitudes Tue–Thu than Sat–Mon. The TRMM radar product 2A23 [*TRMM PR Team*, 2005] reports "storm

Table 1. Parameters of Weekly-Cycle Fits to TMI-Estimated Area-Averaged Rainfall

Region	r_0 [a]	r_7 [a]	ϕ_7 [b]	p
Area A (SW U.S.)	0.129	0.0035	5.4	0.86
Area B (SE U.S.)	0.174	0.025	4.7	0.10
Area C (Coastal Atl.)	0.221	0.042	0.9	0.035
Area D (Atl. East of C)	0.165	0.028	0.6	0.10
Area E (Gulf of Mex.)	0.098	0.016	1.1	0.18

[a]Units: mm h^{-1}.
[b]Time of the week when sinusoidal fit peaks, with $0 \leq \phi_7 < 7$ and $0.0 \rightarrow$ 0000 Saturday.
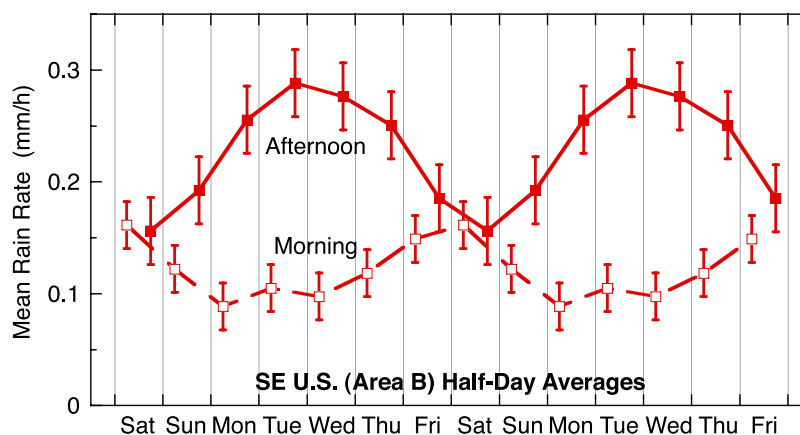
Figure 7. Half-day-average SE-U.S. (area-B) rain rate for mornings (0000–1200 LT) and afternoons (1200–2400 LT). Error bars are 1-sigma confidence limits estimated using resampling.

height" for each radar observation when the PR algorithm determines that precipitation is detected within the radar beam with a high degree of confidence. "Storm height" is the height of the highest point in the radar beam with detectable returns (∼17–18 dBZ), measured relative to mean sea level. The PR beam is roughly 4–5 km in diameter. A detectable radar return indicates the presence of large water droplets or ice particles that have been carried aloft by strong vertical winds. These storm heights are distinct from cloud-top heights, which might be much higher and are not detected by the PR [e.g., *Atlas et al.*, 1995]. There are a number of subtle issues involved in the interpretation of PR storm heights, due to effects such as measurement noise and horizontal tilting of storms, for example, but since we are comparing statistics from different days of the week, these issues are unlikely to change the general conclusions we draw from these statistics.

[37] We collected PR storm-height statistics over the SE U.S. (area B) for JJA 1998–2005. (It is important to note that the PR's coverage extends only slightly above 36 N, so that only the southern half of area B is in fact viewed by the PR. See Appendix B for details.) "Weekend" (Sat–Mon) and "midweek" (Tue–Thu) statistics were obtained separately for morning and afternoon time periods. The number of weekend and midweek PR footprints with valid data (including those with no detectable rain) was 6.8×10^6 each for the morning hours, and 6.6×10^6 each for the afternoon hours. Table 2 gives the fraction of valid PR observations with rain in them for the various cases (i.e., the average areal fraction with rain). It shows that the change in average rainy area from morning to afternoon (an aspect of the diurnal cycle of precipitation) is much smaller on weekends than midweek, consistent with the TMI statistics in Figure 9, which shows that the diurnal cycle is weaker on weekends. It also shows that in the afternoon hours rain is detected about 40% more midweek than on weekends, while in the morning hours rain is detected 20% less.

[38] Figure 10a shows the frequency distributions of storm heights seen by the PR (number of storm heights in 1-km bins expressed as a fraction of the total number of PR footprints with detectable rain), for "weekends" and "midweek" during morning hours. The difference of the weekend distribution from the midweek distribution is indicated

by the dashed curve. It shows that the distribution of midweek storm heights shifts to higher altitudes relative to weekend heights. Figure 10b shows that a similar but much larger change in the distribution occurs during the afternoon hours.

[39] We can calculate the frequency with which storm heights exceed a given altitude a (i.e., the cumulative distribution) by summing the corresponding distribution in Figures 10a and 10b from the highest altitude down to a. The ratio of the midweek cumulative distribution to the weekend distribution then gives the relative probability that midweek storm heights will exceed a given altitude compared to weekend storm heights. The ratios are plotted for morning and afternoon storms in Figure 10c. The probability of afternoon storm heights exceeding 9 km is about 40% higher midweek than on weekends. In other words, not only is the average area covered by afternoon storms 40% higher Tue–Thu compared with Sat–Mon, but, once a storm begins to develop, it is 40% more likely to reach altitudes above 9 km on Tue–Thu than on Sat–Mon. We conjecture that the reason morning storms reach altitudes above 15 km relatively more often than afternoon storms is that the highest storms are also the biggest and longest-lived, and the time for organization at these scales often means that they reach their peak altitudes after midnight and would consequently be counted as "morning" storms in Figure 10.

[40] Deriving confidence limits for the frequency distributions shown in Figure 10 is complicated by the spatial and temporal correlations of storm heights: the counts in a bin cannot be assumed to be independent, except perhaps at the very highest altitudes. If we nevertheless assume that each storm reaches a given height independently of the others, we can estimate confidence limits for the ratios plotted in Figure 10c. The method is described in Appendix A. The "two-sigma" error bars in the plotted ratios are based on this assumption. They are probably too small, especially at lower altitudes, but may provide a helpful perspective about the level of sampling error that may be present in the ratios.

[41] *Petersen and Rutledge* [2001] found that echo-top heights at 30 dBZ are more indicative of changes in convective intensity than is probably the case for ∼17 dBZ reflectivities on which PR storm height is based. It would therefore be desirable to examine the changes in 30-dBZ
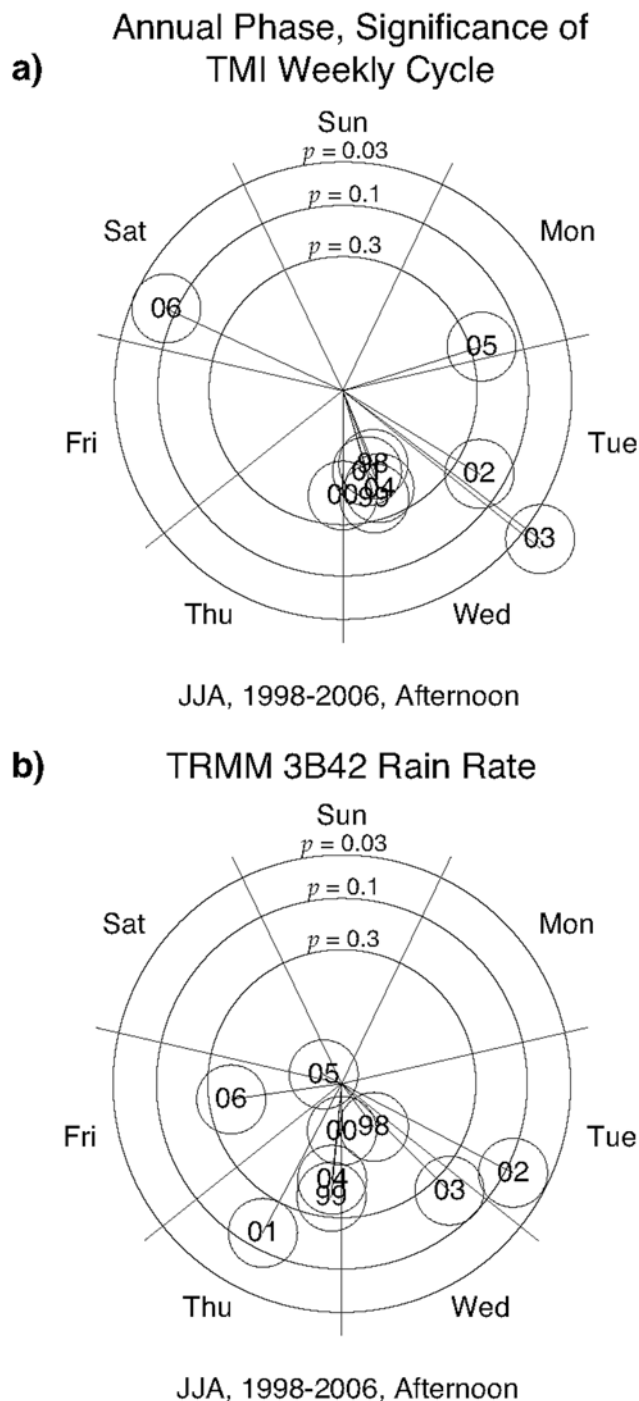
a) Annual Phase, Significance of TMI Weekly Cycle

JJA, 1998–2006, Afternoon

b) TRMM 3B42 Rain Rate

JJA, 1998–2006, Afternoon

Figure 8. Phases and significance levels of weekly cycle fits to average afternoon (1200–2400 LT) rain rate over SE U.S. (area B in Figure 3b) for 9 individual summers for 1998–2006. (a) TMI v. 6 data alone. (b) 3-hourly TRMM merged satellite product (TMPA).

echo-top height statistics to reinforce our conclusion that the midweek increase in storm heights is due to an increase in convective vigor, but it is difficult to think of a physically plausible scenario in which hypothetically weaker midweek storms loft higher reflectivity material above 10 km than

hypothetically stronger weekend storms. For mesoscale convective systems, at least, *Zipser and Lutz* [1994] find that mean reflectivity falls more quickly with altitude for heights above 5 km in the less unstable convective environments over the tropical ocean than in the more unstable environments over land, lending some support to using PR storm height as a qualitative measure of convective vigor.

5. Cycles in Reanalysis and Gauge Data

5.1. Reanalysis Winds

[42] The weekly cycles in areas B and C are strong enough that it would be surprising if there were not corresponding variations in the wind fields over the regions. Using version R-2 of the National Centers for Environmental Prediction/Department of Energy (NCEP/DOE) reanalysis data [*Kanamitsu et al.*, 2002] (referred to here as NCEP2), we obtained wind statistics over areas B and C that seem likely to reflect changes in convective activity in the areas: average surface (1000-hPa) convergence of the horizontal winds, vertical wind at 500 hPa, and horizontal wind divergence at 300 hPa. Note that the daily reanalysis data we use are averages of 6-hourly values from 00Z to 18Z. At typical eastern U.S. longitudes, the data therefore represent averages over roughly 1800 LT the previous day to 1200 LT of the nominal (UT) day of the reanalysis.

[43] Figure 11 shows these reanalysis-wind statistics as a function of the day of the week, derived from summer (JJA) data for 1998–2005. The signal strengths of the weekly cycles over land are very high, as measured by the significance levels p (see figure caption); the cycles over the ocean are noisier. The weekly cycle in air motion represented by these averages corresponds quite well with the behavior one would expect to accompany the convection associated with the rainfall cycles observed by TRMM. Note that for area B the TMI rain rate and all but the 300-hPa divergence have a minimum on Sunday, while for area C all have a minimum on Tuesday, even though the satellite data and the NCEP-reanalysis data use very different measurement systems with very different sampling characteristics.

5.2. Gauge Rainfall, Moisture Convergence

[44] Rain gauges measure rainfall more directly than any remote sensing technique, but only over an area the size of a dinner plate. Since variations in rain rate are spatially correlated, however, measurements by a single gauge reflect changes in rainfall over an area surrounding the gauge, and so a sufficiently dense array of gauges can detect changes in spatially averaged rain rates. The National Climatic Data Center (NCDC) has developed a quality-controlled data set of thousands of rain-gauge records across the U.S. [*Vose et al.*, 1992]. We used their product designated "Data Set 9300" from the Global Historical Climatology Network (GHCN), version 1.0, updated through 2005. The data set we used covers 1901–2005, though the number of gauges begins to diminish steadily as one goes back in time from 1950. [Version 2 of this data set was released after this analysis was completed. See *GHCN*, 2007].

[45] The NCEP reanalysis products include estimates of surface rainfall, but these estimates are more sensitive to model parameterizations than are the wind and vertical
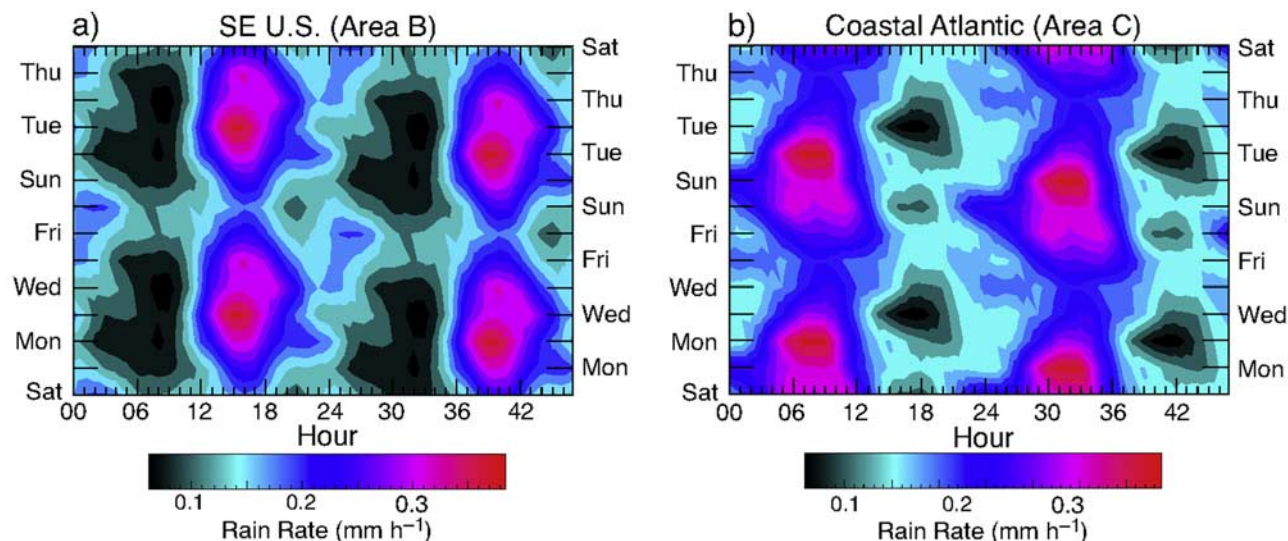
Figure 9. Average TMI-estimated rain rate as a function of the day of the week and hour of the day (local time) using data from June–August, 1998–2005. Hourly values have been smoothed with a "centered" running 4-h average, $r_t = [(1/4)(r_{t-2} + r_{t-1} + r_t + r_{t+1}) + (1/4)(r_{t-1} + r_t + r_{t+1} + r_{t+2})]/2$. Because the day advances by 1 every 24 h, data for hours 00–23 have been repeated for hours 24–47 but assigned to the next day of the week. The right-hand vertical axis is therefore shifted by 1 day relative to the left-hand axis. (a) Averages for area B in Figure 3b. (b) Averages for area C.

humidity profiles [*Kalnay et al.*, 1996]. Because daily variations in vertically integrated moisture convergence on these regional scales should be somewhat representative of daily changes in rainfall (and perhaps ice aloft) in the regions, we have computed the daily averages of column-integrated moisture convergence from the NCEP2 reanalysis data using 6-hourly summer data for 1998–2005. *Roads et al.* [2002] suggest that, despite moisture convergence being a second-order quantity, regional daily vertically integrated convergences computed from 6-hourly model analyses tend to be fairly representative of what more accurate calculations based on each model time step would give. In Figure 12 we plot for each day of the week the difference from the mean of the daily vertically integrated moisture convergence over area B, along with the summertime daily anomalies of TMI rainfall and of the averages (1998–2005) of GHCN gauges in the area (approximately 1800 in number and fairly evenly distributed geographically). Given the level of sampling errors in the moisture convergence anomalies, TMI and gauge rainfall estimates, it would be difficult to distinguish them from one another on a statistical basis.

[46] Table 3 gives the parameters for fits of (1) to the various data and the significance levels *p* of the fits. The negative value of r_0 for moisture convergence indicates that, on average, moisture is exported by the atmosphere from area B during JJA [see for example, *Peixoto and Oort*, 1992, p. 296]. [The rain gauge daily totals are fit to (1) with *t* taking integer values, with $t = 0$ representing Saturday. The value of ϕ_7 given in the table for the fit to the rain-gauge data therefore includes an additional 0.5 day in order to make the comparison with the TMI phase more appropriate. Likewise, because the moisture convergence values for a given day represent averages of estimates for approximately 1800 LT the previous day and 0000, 0600, and 1200 LT for

the given day, the value of ϕ_7 given in the table has been increased by 0.125 day above the phase obtained in the fit.]

[47] The weekly cycle in gauge-measured rainfall is comparable in size and phase to that of the TMI estimates, in the sense that r_7/r_0 for the gauge data is about 75% of the satellite's, and the difference in phases could easily be due to differences in sampling. This suggests that surface rainfall is indeed exhibiting a weekly cycle similar to what the TMI data suggest, though it may not be quite as large as what the TMI estimates indicate.
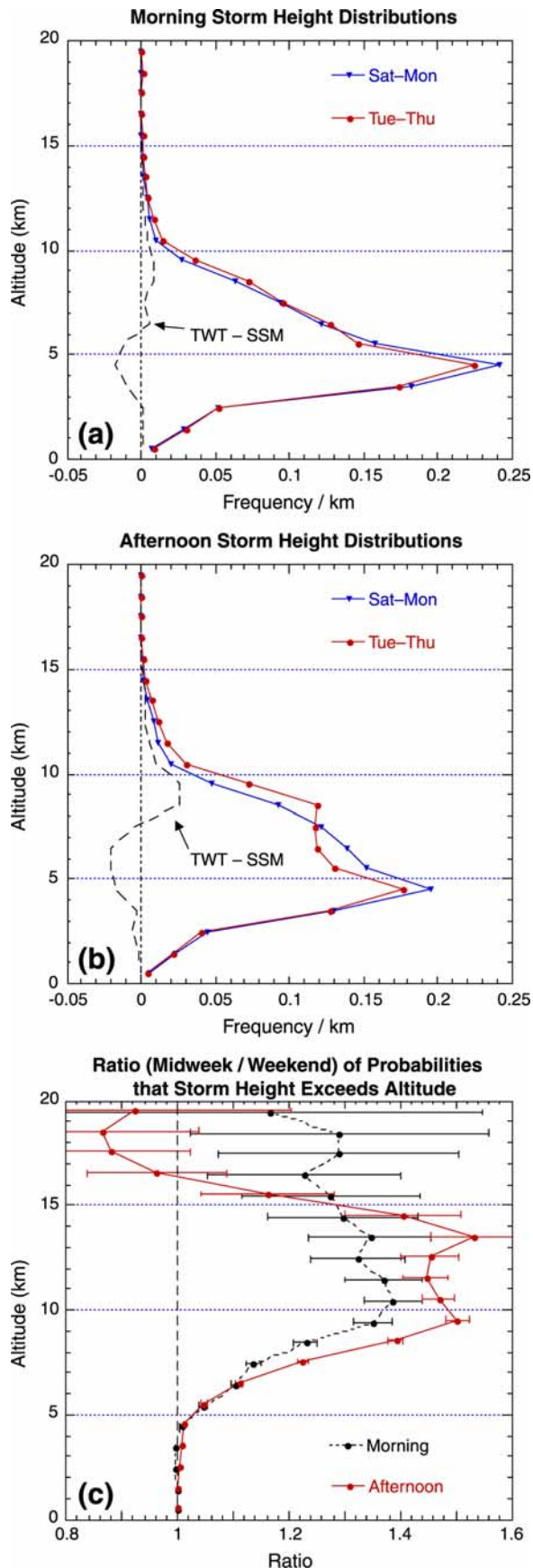
6. Historical Behavior of Weekly Cycle

[48] We have so far looked for weekly cycles in precipitation and other fields during the TRMM era, which started in December 1997. The GHCN rain gauge data extend back to 1901, though coverage dwindles from about 1200 gauges in the later 1940's to about 400 in 1901. The first version of the NCEP-reanalysis data [*Kalnay et al.*, 1996], referred to here as NCEP1, differs from NCEP2 in a number of ways: NCEP2 incorporates a number of adjustments and bug fixes, and, in particular, improves its estimates of soil moisture by using measured surface rain rates where possible rather than the model's own surface rain rates, whereas NCEP1 uses model-generated surface rain rates. NCEP1, on the other hand, covers the longer period 1948–2005;

Table 2. Average Fraction of Area With Rain Seen by PR[a]

	Morning	Afternoon
Sat–Mon	0.0297	0.0415
Tue–Thu	0.0245	0.0579

[a]Fraction of PR footprints identified with high confidence as containing rain, from TRMM PR product 2A23, for morning (0000–1200 LT) and afternoon (1200–2400 LT) hours for weekend and midweek periods, over area B for JJA 1998–2005.

NCEP2 only covers 1979–2005. It is therefore tempting to look for a weekly cycle in these earlier data.

[49] Examining the historical behavior of the strength of the weekly cycle is subject to a number of uncertainties. From a physical perspective, pollution levels and types of pollution have changed with the decades due to changes in regulation, technology, and population. If it is indeed pollution causing most of the weekly cycle we see in the data, we cannot be sure the pollution types of years ago had the same impact as current pollution types are having.

[50] From a statistical perspective, if we confine ourselves to daily averages (rather than to afternoon data), the strength of the signal we have seen in the 8-year period 1998–2005 over area B varies with the quantity examined, with significance levels from $p = 0.01$ to $p = 0.3$ (see caption to Figure 11 and Table 3). If such significance levels are characteristic of the signal in earlier years, then, for example, an examination of ten 8-year periods is almost guaranteed to produce cases with estimated significance levels of $p = 0.1$ even if they are entirely spurious.

[51] The TRMM data suggest that our best hope of learning whether a weekly cycle has been present in earlier years would be to restrict our analysis to afternoon data, since the weekly cycle seems so much stronger in the afternoon data. The NCEP-reanalysis data are in fact available at 6-hourly intervals, seeming to offer us a chance to look at atmospheric behavior for afternoon hours alone. When we looked at NCEP-reanalysis data for 00Z (corresponding to "the afternoon," about 1800 LT over the SE U.S.) and 12Z (corresponding to about 0600 LT) results seemed generally to be consistent with what the TRMM data lead us to expect for the last decade, but are not so easy to interpret for earlier decades. Since the NCEP data assimilation relies heavily on radiosonde data that are supplied at best only twice per day, and the models themselves have some difficulty in representing the diurnal cycle of convective behavior [e.g., *Janowiak et al.*, 2007], it is possible that current data assimilation products are not yet suited to our needs. Rain-gauge data at hourly intervals may be able to help here, but requires analysis of an order of magnitude more data than we have looked at so far, and we have not done this yet.

[52] With these caveats in mind, we present a few examples of what we see for the historical behavior of the weekly cycle in rain-gauge and NCEP-reanalysis data. We use the signal-to-noise ratio r_7/σ_7 to represent the strength of the weekly cycle, with the quantity σ_7 defined in

Figure 10. Frequency statistics of PR storm heights over area B using 1-km-altitude bins, derived from TRMM PR product 2A23, v. 6. (a) Morning (0000–1200 LT) storm heights. Circular dots show the distribution of "midweek" storm heights, while triangles show "weekend" distribution. Dashed curve shows the difference. (b) Afternoon (1200–2400 LT) storm heights. (c) Ratio of midweek cumulative distributions to weekend cumulative distributions, representing the relative probability that midweek storm heights exceed weekend heights, with two-sigma error bars (see text for caveats). (Cumulative distributions defined as integrals of the probability distributions from the highest altitude downward).
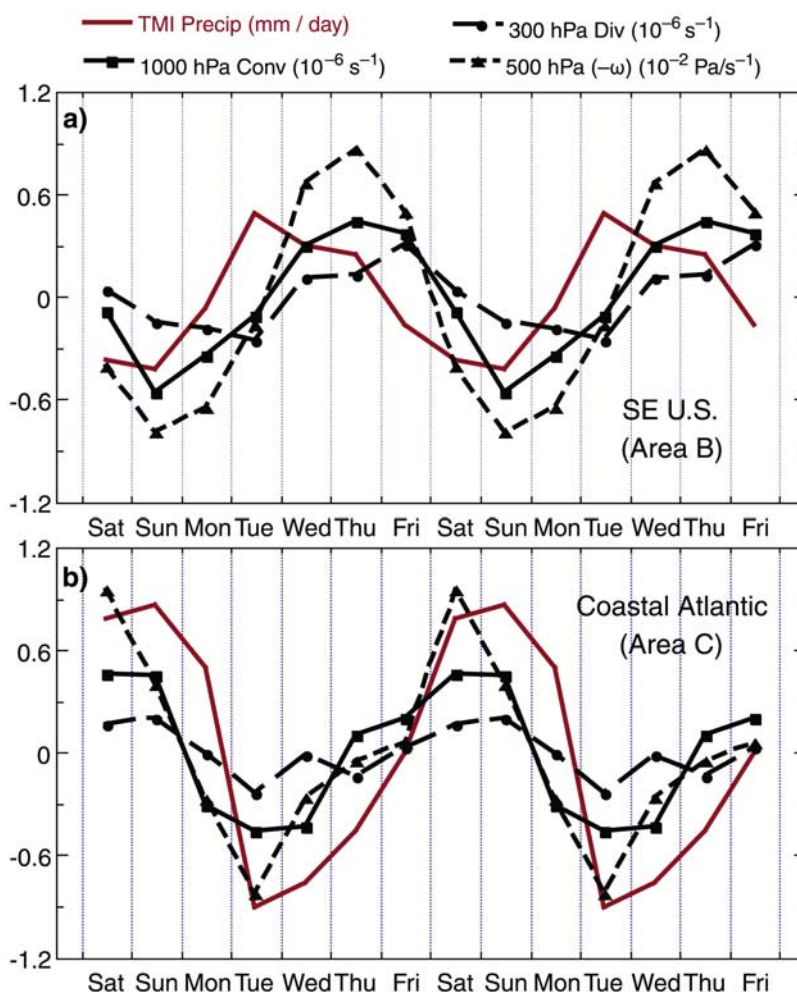
Figure 11. Wind field statistics (summer, 1998–2005) from NCEP2 reanalysis over areas B and C in Figure 3b as a function of the day of the week. (Daily reanalysis statistics represent averages from 1800 LT the previous day to 1200 LT of the plotted day.) Average wind convergence over the area at 1000 hPa indicates net inflow into the area near the surface. Average divergence at 300 hPa indicates net export of air out of the area at altitudes typical of storm tops. Mid-atmosphere average vertical velocity at 500 hPa is represented by $-\omega$, the time rate of change of air pressure of an air parcel (sign reversed). Daily TMI anomalies, based on Figure 4a, are superimposed for comparison. Differences from time means are plotted for each quantity. Statistical significance levels for the 3 wind fields for area B are $p = 0.024$, 0.045, and 0.011, respectively; for area C they are $p = 0.047$, 0.41, and 0.20.

Appendix A representing the estimated sampling variability in the weekly-amplitude parameter r_7, from which the significance level p can be obtained using the formula $p = \exp[-(r_7/\sigma_7)^2]$. [A plot of σ_7 for the area-B rain-gauge average for each year (not shown) is fairly constant, and does not rise in the earlier years as might be expected if the decline in the number of gauges for years prior to 1950 caused the representativeness of the area average to diminish with the number of gauges.]

[53] Figure 13a shows the signal-to-noise ratio of weekly-cycle fits for daily area-averaged gauge data over area B, plotted as far back as 1908. The statistics of fits plotted at year y are based on the 8 years $y-7$ to y, using only the summer data. We have chosen an 8-year window solely because it is the size of the window used in the TRMM studies in the earlier sections of this paper. Different windows can produce significantly different-looking plots.

(One example is shown later.) Two horizontal lines are drawn on the plot indicating the values of r_7/σ_7 for which $p = 0.5$ and 0.05. If there were no weekly cycle, we would expect half the ratios to fall below $p = 0.5$ and half to fall above it. We would expect 5% of the ratios to exceed the $p = 0.05$ level by accident. The figure suggests that a weekly cycle might have begun increasing to detectable levels in the 1980's, but this is far from clear. The day of the week ϕ_7 when the weekly fit peaks is plotted in Figure 13b. Note that the phase of the fits becomes more erratic for low signal-to-noise ratios (e.g., year 2001 in Figure 13).

[54] There is a hint in Figure 13 that a weekly cycle might have appeared in the decades around 1940, peaking Sunday/Monday, then diminished and reappeared in the late 1970's with a peak closer to the middle of the week. It is possible that this might be related to the changes in the composition of air pollution over these decades from absorbing to less
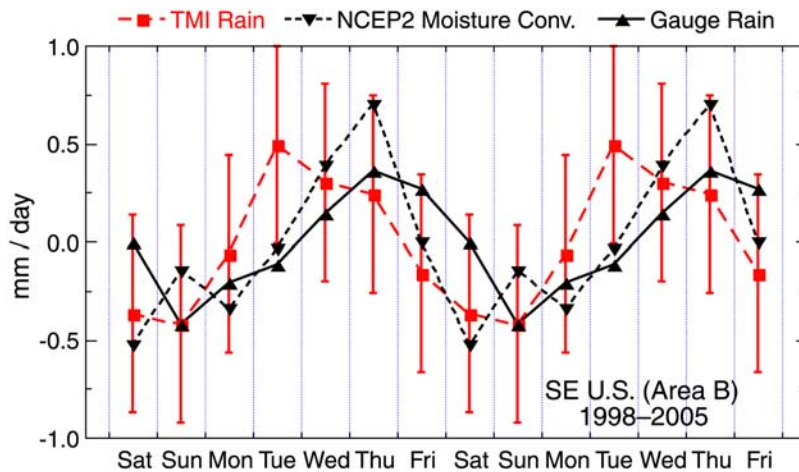
Figure 12. Daily anomalies of rain-gauge averages and of vertically integrated NCEP2 moisture convergence over area B, with TMI rain estimates superimposed. (Daily moisture convergence values represent averages from 1800 LT the previous day to 1200 LT of the plotted day.) Error bars (1-sigma) for the TMI estimates are estimated using resampling, as described in Appendix A. Parameters of fits in Table 3.

absorbing aerosols: *Lefohn et al.* [1999] suggest that sulfur emissions in the U.S. might have stabilized beginning around 1920, possibly due to the impact of government regulatory action, while *Novakov et al.* [2003] suggest that black carbon emissions from diesel engines began to rise in the 1950's while black carbon emissions from other sources decreased. Diesel particles are generally smaller than 100 nm. Their optical cross section is very small, but they are still very active as cloud condensation nuclei (CCN) when chemically mature [*Dusek et al.*, 2006]. This suggests that there might have been a transition from large absorbing aerosols during the first half of the 20th century to less absorbing, smaller and more numerous particles toward the end of the century. Absorption by aerosols reduces solar heating of the surface and hence suppresses convection [*Koren et al.*, 2004], while the CCN activity of aerosols enhances deep convection [*Rosenfeld*, 2006]. This can potentially explain a transition from a weekly cycle that is dominated by aerosol absorption suppressing midweek convection in the middle of the 20th century to the period toward the end of the 20th century in which the elimination of visible black smoke causes a changeover to midweek intensification due to the increasing number of small, sub-visible CCN along with decreasing solar absorption by the aerosols [*Wild et al.*, 2005].

[55] Figure 14 shows the signal-to-noise ratios and phases for NCEP1 surface wind convergence, 300-hPa wind divergence, and 500-hPa vertical velocity with an 8-year running window. (Phases have been increased by 0.125 days in an attempt to take into account the facts that days are represented as integers, daily averages are based on 00Z, 06Z, 12Z, and 18Z, and local time over area B is about 6 h earlier than UT.) There appears to be a tendency for the weekly signal to begin strengthening in the 1980's in all plots. This tendency appears much more dramatic when a window longer than the 8-year window used in Figures 13–14 is used: Figure 15 shows the signal-to-noise ratios for running 15-year fits to the gauge and NCEP1 reanalysis wind fields

(again, NCEP1 averages assigned to a given day represent averages from 1800 LT the previous day to 1200 LT that day). It should be noted that the NCEP1 reanalysis incorporated TIROS (Television Infrared Observation Satellite) Operational Vertical Sounder (TOVS) data beginning in about 1979 [*Kalnay et al.*, 1996], and it is conceivable that this might have increased the signal-to-noise ratio of a weekly cycle relative to what could be observed prior to 1979. Such a change would not affect the rain-gauge data, however.

7. Discussion

[56] Daily rainfall estimated by the TMI appears to have a significant weekly cycle over the SE U.S. (area B in Figure 3b). Its amplitude r_7 is about 14% of the mean r_0. Rain-gauge data suggest that the weekly cycle in surface rainfall might be somewhat smaller in amplitude, perhaps 11% of the mean. Statistical tests that take account of natural variability with multiday timescales indicate that the weekly cycles in both morning and afternoon TMI estimates of rain rate and in reanalysis estimates of atmospheric winds over the SE U.S. are extremely unlikely to be accidents of natural variability. Figure 4a shows that average TMI rain rate over the SE U.S. is largest during the middle of the week and drops to its

Table 3. Statistics of Fits to Various Rainfall Estimates[a]

	TMI Precip	Rain Gauges	Moisture Convergence
r_0	4.18	3.31	−2.21
r_7	0.60	0.35	0.48
σ_7	0.40	0.22	0.40
ϕ_7	4.7	5.6	4.6
p	0.101	0.089	0.25

[a]Parameters of sinusoidal fits to rain-rate estimates from TMI, GHCN rain gauges, and NCEP2 reanalysis vertically integrated moisture convergence, averaged over area B. Parameters r_0, r_7, and σ_7 have units mm/day. Sinusoidal fit peaks on day ϕ_7, $0 \leq \phi_7 < 7$, with $0.0 \rightarrow 0000$ Saturday.
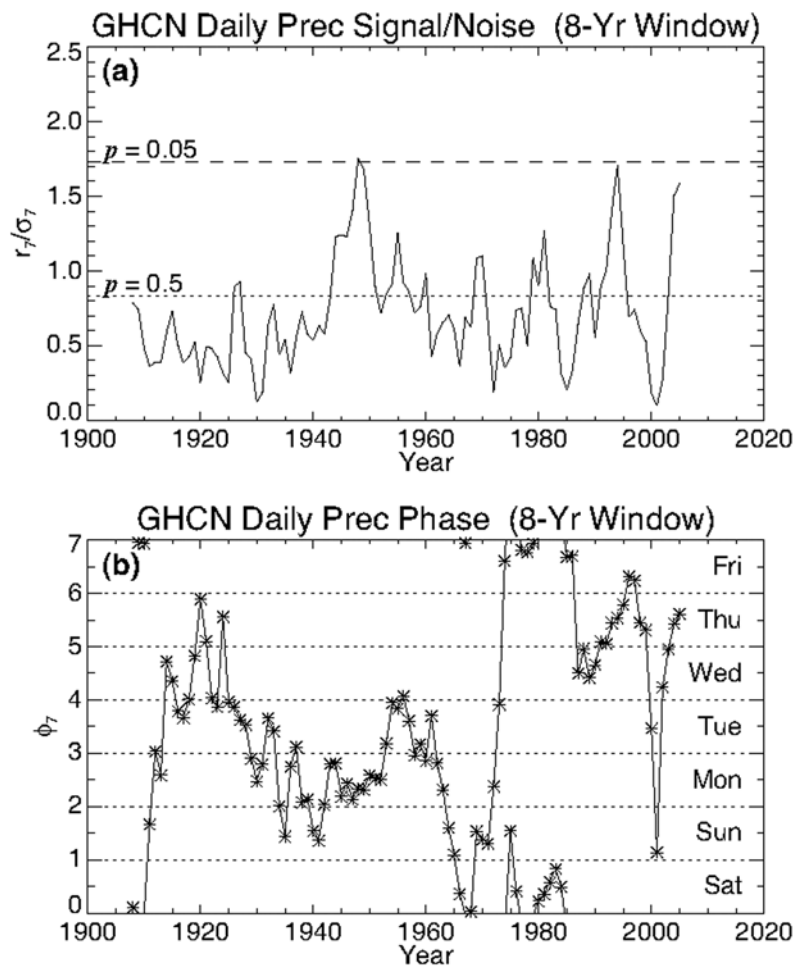
Figure 13. Statistics of weekly-cycle fits to area-B-averaged GHCN rain-gauge data, based on fits to 8 consecutive summers of data ending on the year plotted. (a) Plot of signal-to-noise ratios r_7/σ_7 (see text for explanation of horizontal lines labeled with p); (b) phases ϕ_7 of fits.

lowest value on Sunday—behavior very similar to anthropogenic pollution.

[57] Correlation does not prove causation, however. There are other types of human activity not directly contributing to air pollution that vary on a weekly basis and that might affect storm dynamics. The heat produced in powering motor vehicles, industrial activity, and generating electricity is too small to affect circulation on this scale. Jet contrails may be more numerous on weekdays, but would tend to reduce afternoon thermal instability rather than increase it. Irrigation of fields might have a weekly cycle, but it seems unlikely that this would change the available water in the atmosphere enough to account for the large changes in afternoon rainfall over the SE U.S. Over the drier SW U.S., where irrigation practices are more likely to affect atmospheric moisture content, a weekly cycle is not detectable. Other possibilities are discussed by *de F. Forster and Solomon* [2003].

[58] These considerations suggest that summertime (mostly convective) rain amounts are increased, at least on large scales, by the increase in the kinds of pollution that vary with the day of the week because of human activity. The direct radiative effects of aerosols are unlikely to be responsible, since aerosols tend to reduce surface solar heating [*Ramanathan et al.*, 2001; *Koren et al.*, 2004]; their radiative effects would tend to decrease midweek afternoon rainfall, in contrast with the observations. It is possible that concentrations of radiatively absorptive aerosols like black carbon could alter the vertical distribution of heating and help initiate elevated convection in extreme cases of heavy black smoke [*Rudich et al.*, 2003]. Such clouds would be typically weaker than those starting from the boundary layer, however, and *Koren et al.* [2004] showed that the suppression effect on the triggering of convection dominates the heating effect. It is therefore difficult to see how the heating due to aerosol absorption would explain the observed changes in the distribution of storm heights seen in section 4. This would, however, explain the mid-20th-century reversal of the weekly cycle, when the absorptive properties of the aerosols probably began to weaken while the CCN number concentration probably continued to increase. On balance, based on what is known about the effect of aerosols on droplet formation in developing storms and on recent modeling studies, we believe the most likely explanation of the changes we have observed during the last few decades is the one proposed in the Introduction.
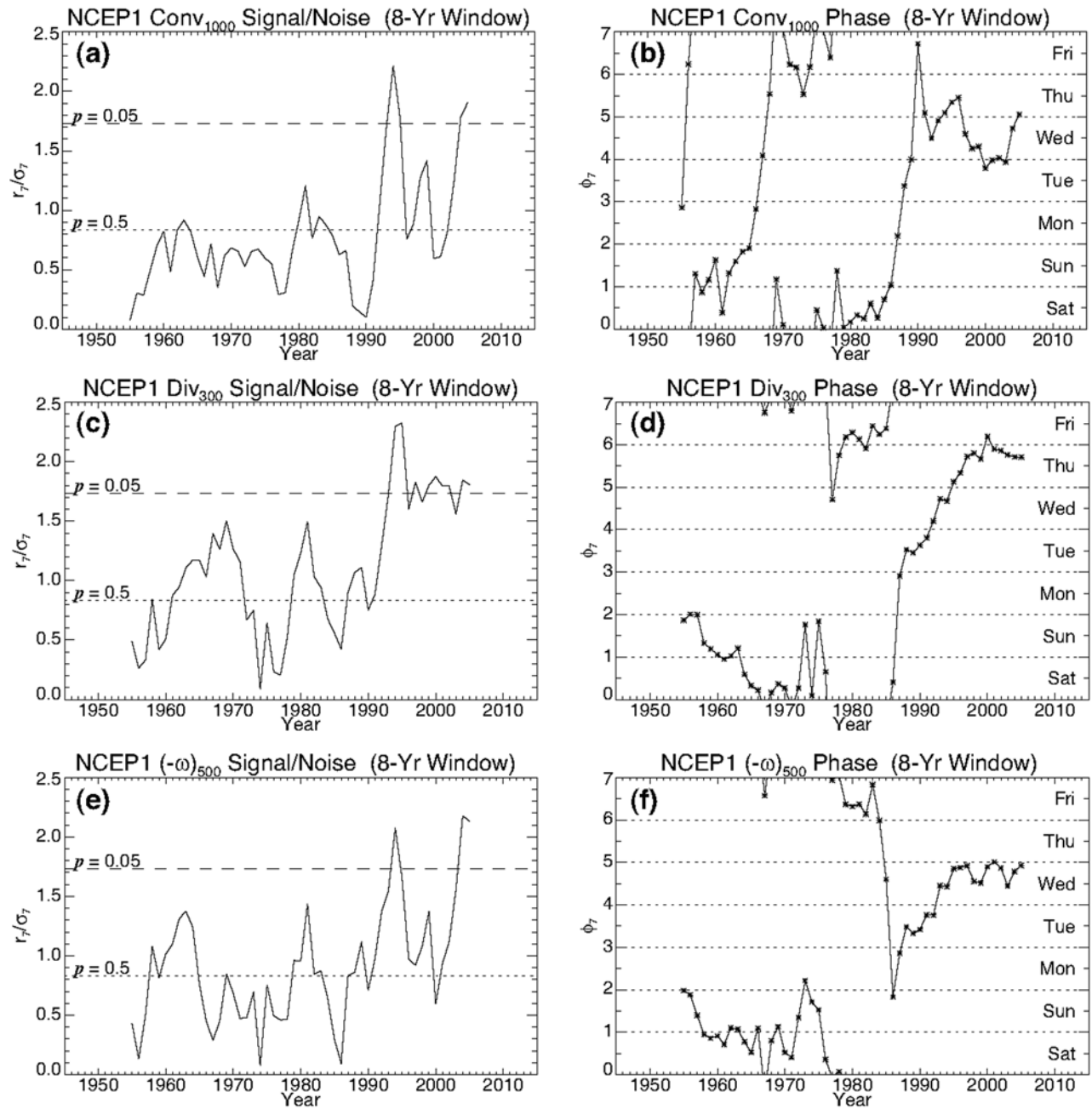
Figure 14. As in Figure 13, but showing statistics of weekly-cycle fits to area-B-averaged NCEP1-reanalysis 1000-hPa horizontal-wind convergence (panels a, b), 300-hPa horizontal-wind divergence (panels c, d), and 500-hPa vertical wind ($-\omega$) (panels e, f).

[59] The weekly cycle in the Atlantic off the east coast of the U.S. (area C) is remarkable in that it is almost exactly opposite in phase to the cycle over the nearby land, and quite strong; see, in particular, Figure 9. Though it is not possible with the amount of data at hand to provide a definitive explanation for this, we offer a tentative interpretation based on the following observations:

[60] 1) As mentioned above, pollution aerosols tend to reduce cloud droplet size, suppress early warm rainout and enhance the subsequent mixed-phase precipitation. Sea-salt aerosols restore much of the warm rain in polluted clouds

and hence weaken the pollution effects over ocean, but do not reverse them [*Rosenfeld et al.*, 2002].

[61] 2) Over water, the TMI senses rain much more directly than over land, and is less sensitive to ice aloft. Suppression of the conversion of cloud drops to raindrops should not affect the TMI signal much because it is dominated by the amount of cloud and rainwater combined and not very sensitive to their partitioning.

[62] These two considerations make it difficult to explain the observed midweek diminution of TMI rainfall over area C as a direct consequence of weekly variations in pollution in the area. Furthermore, we note that the weekly signal
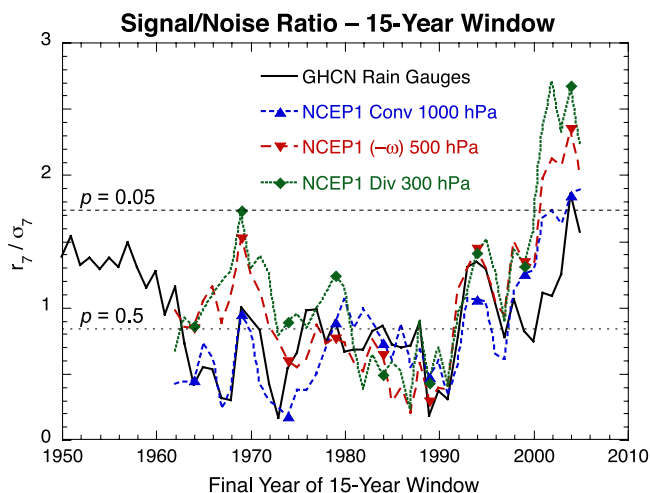
Signal/Noise Ratio – 15-Year Window

Figure 15. Signal-to-noise ratios r_7/σ_7 of weekly-cycle fits to area-B-averaged summer GHCN gauge data and NCEP1 reanalysis estimates of surface wind convergence, 500-hPa vertical wind velocity, and 300-hPa wind divergence using a 15-year window. Value plotted for year y represents fit to years $y - 14$ to y.

over land appears to die out near the coast and to reverse sign and become very strong over the open water. The phase does not seem to drift significantly to later times as one moves further eastward, which might have been expected if the suppression is due to pollution emanating from the continent. (CB report that they saw a steadily increasing delay in peak rainfall in the oceanic areas further and further east of area C, based on their all-season statistics. The almost simultaneous peak we see in the rainfall over area D in Figure 5a does not seem to be consistent with this, however. We examined the rainfall over an area east of D and adjacent to it: it has a slight weekly cycle, but its phase is not statistically distinguishable from that of the two oceanic areas C and D).

[63] These facts suggest to us that what we are in fact seeing is dynamical suppression of midweek precipitation over the ocean in response to the invigorated convection over the land, as air pumped into the upper troposphere over the continent descends over the surrounding oceanic area, suppressing convection there and reducing its coverage and intensity. This is, in essence, a monsoon-like modulation of the land-ocean circulation in response to the aerosol-induced changes in convection. Validating our proposed explanation will require quantitative model simulations of how changes in convection over the continent might affect offshore convection, and satellite documentation of the weekly cycle of pollution over the ocean.

[64] *Bäumer and Vogel* [2007] point out that the weekly cycles they see in various variables do not seem to correlate well with likely local aerosol changes (they do not provide data for actual aerosol levels) inferred from the proximity of urban areas to the stations they studied, and suggest that what they might be seeing is a regional rather than local effect. (It should be noted that they studied all-season averages, whereas we have presented statistics only for the summer season, and the physical mechanism proposed

here is likely only to be applicable to summer convection. It is therefore difficult to make detailed comparisons of their results and ours.) It is worth noting that if the effects of a weekly cycle in one locality can induce very different weekly cycles in nearby areas, as we have suggested may be occurring over the coastal Atlantic near the U.S., then local weekly cycles in precipitation may not be governed solely by local changes in pollution.

8. Conclusions and Questions

[65] Based on summertime TRMM satellite, gauge, and reanalysis data, we have presented evidence that

[66] 1) both the average area and intensity of TMI-estimated rain are greater in the middle of the week than on weekends over a substantial portion of the southeast U.S.;

[67] 2) the increase in afternoon rainstorm activity during the middle of the week relative to weekends is statistically highly significant;

[68] 3) there is a strong tendency for this weekly variation to show up in afternoon data in most (but not all) summers;

[69] 4) the TRMM radar sees the area with rain increase during the middle of the week, and hydrometeors reach higher altitudes more often, compared with weekends;

[70] 5) the effect, which clearly must be anthropogenic, extends over the nearby Atlantic, and is almost as strong there, but is reversed in sign;

[71] 6) there are weekly changes in lower-level wind convergence, upper-level divergence and mid-level vertical velocities over the southeast U.S., along with compensatory changes in the corresponding quantities over the nearby ocean, that are physically consistent with the changes in convection implied by the satellite rain estimates;

[72] 7) both gauge and reanalysis moisture-convergence data are consistent with the satellite observations; and

[73] 8) a weekly cycle in the drier western half of the U.S., if present, is weak.

[74] Based on the substantial amount of research documenting the influence of aerosols on cloud development and the weekly variation in aerosol concentrations, this evidence strongly suggests that air pollution invigorates storms in areas with large vertical instability, such as occurs over land in the summer, when there is an ample supply of moisture. The enhanced convection is sufficiently vigorous that it may suppress convection in neighboring oceanic areas. The observations are consistent with the dynamical picture presented by Rosenfeld in the works of *Williams et al.* [2002] and *Andreae et al.* [2004] as well as with some recent model studies. The weekly cycle in rainfall thus seems to provide an opportunity for investigating the larger-scale climate implications of this picture.

[75] Many questions are raised by these results:

[76] 1) Which constituents of air pollution are responsible for the rainstorm invigoration?

[77] 2) Does the invigoration occur more around large urban areas or over rural areas? (*Wang* [2005], finds that the aerosol effect on model storm development tends to saturate at high concentrations, suggesting that storm intensification might be most noticeable in rural areas.)

[78] 3) Is there a weekly cycle in rainfall in areas of the U.S. not visible to TRMM? Are there other areas in the

world where a weekly cycle in rainfall would be expected? (Many areas do not seem to have strong weekly cycles of pollution. See *Beirle et al.* [2003], for example. Moreover, the absorbing aerosols in the most polluted regions of the world might neutralize or even reverse the CCN invigoration effect.)

[79] 4) Is some part of the intensification of rain events during the past 30 years reported by *Groisman et al.* [2004] due to decadal changes in aerosol absorption and CCN activity rather than the climatic effects of greenhouse gases? If weekly changes in human activity affect storm behavior, decadal trends in the same activities are likely to produce corresponding trends in storm behavior.

[80] 5) Since air pollution is scavenged by rain, and rain appears to be increased by pollution (in the environments dealt with here), the weekly cycle we observe is a complex product of these interactions and emissions. Can atmospheric models that incorporate aerosol effects reproduce the observed weekly cycle?

[81] 6) Can atmospheric models reproduce (and help us understand) the day/night differences in the weekly cycle observed over the SE U.S.?

[82] 7) More generally, how do aerosols affect the diurnal cycle of rainfall?

[83] 8) Can atmospheric models reproduce the seesaw relationship of the weekly cycle over land and over the nearby ocean?

[84] 9) If there is a "weekend effect" on storm development, how much error is made in forecasts of precipitation and severe weather if forecast models do not include aerosol effects?

Appendix A: Estimation of Statistical Significance of Weekly Cycles

[85] The likelihood that a weekly cycle seen in the data is an accident of natural variations in rainfall, which, of course, are very unlikely to favor any day of the week, has been estimated in two ways, both of which proved to give similar values for the statistical significance level of the observed cycles: The first method is based on one described by *Bell and Reid* [1993], and involves estimating the sampling error in a sinusoidal fit to the weekly cycle specified in equation (1). The time series is broken into 7-day chunks, each of which is fit to the linear version of Equation (1) with 3 unknown amplitudes,

$$r(t) = r_0 + c_7 \cos(\omega_7 t) + s_7 \sin(\omega_7 t) \quad (A1)$$

with $r_7^2 = c_7^2 + s_7^2$ and $\phi_7 = (7/2\pi)\arctan(s_7/c_7)$. If n weeks of data are available and provide n estimates of the coefficients c_7 and s_7, then the error variance in c_7 and s_7 is estimated as the variance of the n estimates divided by n, assuming that the amplitudes are not very correlated from week to week. Under the null hypothesis $r_7 = 0$, r_7^2 is distributed for large n as a chi-square variable with 2 degrees of freedom, and the probability that r_7 exceeds R by accident is given by

$$\text{Prob}(r_7 > R) = \exp\left(-R^2/\sigma_7^2\right) \quad (A2)$$

with $\sigma_7^2 = [\text{var}(c_7) + \text{var}(s_7)]/n$. As pointed out, for example, by *Langmuir* [1953] (p. 89) or *Collier and Bowman* [2004], if n is not large, it is more appropriate to use the Fisher F probability distribution, which takes into account the fact that σ_7^2 is estimated from a finite number of samples (n weeks), and gives, for this particular case,

$$\text{Prob}(r_7 > R) = \left[1 + \left(R^2/\sigma_7^2\right)/n'\right]^{-n'} \quad (A3)$$

with $n' = n - 1$.

[86] The second method we use is a bootstrap (resampling) approach that generates artificial (resampled) time series from randomly chosen chunks of data while attempting to preserve the time correlation in the data [e.g., *Wilks*, 1997]. Resampling was carried out by using the original time sequence of observations, dividing it into chunks of lengths 4, 5, or 6 days (randomly chosen for each chunk) and replacing each chunk with another of the same length randomly selected from those segments of the data whose local times of observation are within 2 h of the chunk being replaced. This preserves the effects of the diurnal cycle of rainfall in the statistics, but scrambles any associations with the day of the week. A set of 10,000 synthetic time series and the associated fit parameters $r_7^{(\alpha)}$ and $\phi_7^{(\alpha)}$, $\alpha = 1, \ldots,$ 10,000, were obtained. The fraction of fits $r_7^{(\alpha)}$ larger than the observed amplitude r_7 for the actual data was used to estimate the probability p that the observed amplitude could occur by accident, under the null hypothesis that there is no real weekly cycle. The value of σ_7 when resampling is used to estimate p is assigned the value

$$\sigma_7 = r_7(-\ln p)^{-1/2}. \quad (A4)$$

The variances of daily averages across these synthetic series were also used to estimate the error bars for area B in Figures 4, 7, and 12.

[87] The error bars in Figure 10c for the ratio of cumulative distributions of storm heights were estimated assuming that the counts $n(a)$ of how many storm heights exceed altitude a are counts of individual, independent events. If the total count of storm height values is, by definition, $N = n(0)$, then the cumulative distributions $c_i(a)$ whose ratios are plotted in Figure 10c are given by $c_i(a) = n_i(a)/N_i$, where i denotes either weekend (Sat–Mon) or midweek (Tue–Thu), and the ratios plotted are $c_{\text{TWT}}(a)/c_{\text{SSM}}(a)$. The assumption that the counts $n_i(a)$ are independent is certainly not true for low altitudes, but at the highest altitudes the counts are relatively small and the assumption is more reasonable. Denote expectations by angular brackets and write the observed counts $n_i(a)$ as

$$n_i(a) = \langle n_i(a) \rangle + \delta n_i(a), \quad (A5)$$

where $\delta n_i(a)$ is the deviation from the expected mean due to the finite sample size. Because the counts are independent, n_i (we omit specifying a henceforward) is Poisson distributed, with variance

$$\text{var}(n_i) = \text{var}(\delta n_i) = \langle n_i \rangle. \quad (A6)$$

Then we can approximate sampling error in the ratio as

$$\delta(c_{\text{TWT}}/c_{\text{SSM}}) \approx \langle c_{\text{SSM}} \rangle^{-1} \delta c_{\text{TWT}} - \langle c_{\text{TWT}} \rangle \langle c_{\text{SSM}} \rangle^{-2} \delta c_{\text{SSM}} , \tag{A7}$$

from which it follows that the error variance is given by

$$\text{var}(c_{\text{TWT}}/c_{\text{SSM}}) \approx \langle c_{\text{SSM}} \rangle^{-2} \text{var}(\delta c_{\text{TWT}}) + \langle c_{\text{TWT}} \rangle^2 \langle c_{\text{SSM}} \rangle^{-4} \\ \cdot \text{var}(\delta c_{\text{SSM}}). \tag{A8}$$

We have neglected the covariance term $\langle \delta c_{\text{SSM}} \delta c_{\text{TWT}} \rangle$ because the cumulatives are from different days of the week.

[88] Expression (A8) for the variance of the cumulative-distribution errors δc_i can be estimated using

$$\delta c_i \approx \langle N_i \rangle^{-1} \delta n_i - \langle n_i \rangle \langle N_i \rangle^{-2} \delta N_i \tag{A9}$$

and

$$\text{var}(\delta c_i) = \langle (\delta c_i)^2 \rangle. \tag{A10}$$

Substitute Equation (A9) into (A10). Use $\text{var}(\delta N_i) = \langle N_i \rangle$ and $\langle \delta n_i \delta N_i \rangle = \langle (\delta n_i)^2 \rangle = \langle n_i \rangle$, based on the Poisson assumption and the fact that N_i includes the counts in n_i by definition. The variance of c_i is then given by

$$\text{var}(\delta c_i) = c_i^2 \left(n_i^{-1} - N_i^{-1} \right), \tag{A11}$$

where we have replaced the expectations $\langle n_i \rangle$ by their best estimates n_i. Substituting this into Equation (A8) gives us our estimate of the standard deviation of the sampling error in the ratio, $[\text{var}(c_{\text{TWT}}/c_{\text{SSM}})]^{1/2}$.

Appendix B: TRMM Sampling Issues

[89] Because TRMM visits a grid box several days in a row within the same hour of the day, then visits the box for several days about one hour earlier, etc. [e.g., *Negri et al.*, 2002], there is some danger that the satellite might, for example, have a tendency to overfly an area on weekends in the afternoon while visiting the area during the middle of the week in the morning. In other words, the diurnal variation of rainfall might induce a spurious weekly cycle in the TRMM statistics. This possibility has been ruled out by examining the number of TRMM observations of the areas in Figure 3b as a function of both the day of the week and the hour of the day: all hours of the day are about equally observed each day of the week. We have also tried replacing the actual time series of area-averaged rain rate with an artificial diurnal cycle characteristic of the area and found that the spurious weekly cycle induced by the diurnal cycle is two orders of magnitude smaller than the observed weekly cycle. Note, too, that an orbit-induced weekly cycle ought to have shown up in the southwest-U.S. area-A statistics, and it does not.

[90] TRMM's orbital altitude was increased from 350 km to 402.5 km in August 2001 to conserve its remaining fuel. Changes in rain statistics after the boost are subtle, and

unlikely to affect the amplitude or phase of the weekly cycles seen in the data.

[91] TRMM's orbital plane is inclined 35° with respect to the Equator, and as a consequence the TMI and PR instruments view, respectively, latitudes around 31° and 34° roughly 3 times as often as they do equatorial latitudes [e.g., *Bell et al.*, 1990]. TMI coverage extends only up to about 38.4° latitude, and the PR only just beyond 36° (prior to TRMM's orbital boost). Spatial averages of TMI and PR data used here are numerical averages over individual fields of view of the instruments, and so are weighted most heavily toward the best observed latitudes, unlike the spatial averages of gauge and reanalysis data. This choice in averaging was guided by the fact that if a weekly cycle in rainfall was present at equal levels everywhere in an area, then frequency-weighted averaging would produce the highest signal-to-noise ratio. This difference in weighting of the satellite and the gauge and reanalysis data might in principle make comparisons of the averages difficult, but in an experiment we conducted in which the rain gauge data were averaged with weights proportional to the TMI sampling frequency we found little change in the gauge results when compared to those with equal weighting of all gauges.

References

Albrecht, B. A. (1989), Aerosols, cloud microphysics and fractional cloudiness, *Science*, 245, 1227–1230.

Andreae, M. O., D. Rosenfeld, P. Artaxo, A. A. Costa, G. P. Frank, and K. M. Longo (2004), Smoking rain clouds over the Amazon, *Science*, 303(5662), 1337–1342.

Atlas, D., S. Y. Matrosov, A. J. Heymsfield, M.-D. Chou, and D. B. Wolff (1995), Radar and radiation properties of ice clouds, *J. Appl. Meteorol.*, 34, 2329–2345.

Bae, M.-S., J. J. Schauer, J. T. DeMinter, and J. R. Turner (2004), Hourly and daily patterns of particle-phase organic and elemental carbon concentrations in the urban atmosphere, *J. Air Waste Manage. Assoc.*, 54, 823–833.

Bäumer, D., and B. Vogel (2007), An unexpected pattern of distinct weekly periodicities in climatological variables in Germany, *Geophys. Res. Lett.*, 34, L03819, doi:10.1029/2006GL028559.

Beirle, S., U. Platt, M. Wenig, and T. Wagner (2003), Weekly cycle of NO2 by GOME measurements: A signature of anthropogenic sources, *Atmos. Chem. Phys.*, 3, 2225–2232.

Beirle, S., U. Platt, and T. Wagner (2004), Monitoring nitrogen oxides with satellite instruments: High resolution maps from GOME narrow swath

mode and SCIAMACHY, in *Proc. ENVISAT and ERS Symposium, 6–10 September 2004, Salzburg, Austria*, ESA publication SP-572.

Bell, T. L., and N. Reid (1993), Detecting the diurnal cycle of rainfall using satellite observations, *J. Appl. Meteorol*, 32(2), 311–322.

Bell, T. L., A. Abdullah, R. L. Martin, and G. R. North (1990), Sampling errors for satellite-derived tropical rainfall: Monte Carlo study using a space-time stochastic model, *J. Geophys. Res.*, 95D, 2195–2205.

Betts, A. K., and C. Jakob (2002), Study of diurnal cycle of convective precipitation over Amazonia using a single column model, *J. Geophys. Res.*, 107(D23), 4732, doi:10.1029/2002JD002264.

Blanchard, C. L., and S. J. Tanenbaum (2003), Differences between weekday and weekend air pollutant levels in southern California, *J. Air Waste Manage. Assoc.*, 53(7), 816–828.

Cehak, K. (1982), Note on the dependence of precipitation on the day of the week in a medium industrialized city, *Arch. Met. Geoph. Biokl.*, B30, 247–251.

Cerveny, R. S., and R. C. Balling Jr. (1998), Weekly cycles of air pollutants, precipitation and tropical cyclones in the coastal NW Atlantic region, *Nature*, 394, 561–563.

Charron, A., and R. M. Harrison (2005), Fine ($PM_{2.5}$) and coarse ($PM_{2.5-10}$) particulate matter on a heavily trafficked London highway: Sources and processes, *Environ. Sci. Technol.*, 39, 7768–7776.

Cleveland, W. S., T. E. Graedel, B. Kleiner, and J. L. Warner (1974), Sunday and workday variations in photochemical air-pollutants in New Jersey and New York, *Science*, 186(4168), 1037–1038.

Collier, J. C., and K. P. Bowman (2004), Diurnal cycle of tropical precipitation in a general circulation model, *J. Geophys. Res.*, 109, D17105, doi:10.1029/2004JD004818.

de F. Forster, P. M., and S. Solomon (2003), Observations of a "weekend effect" in diurnal temperature range, *Proc. Natl. Acad. Sci.*, 100(20), 11,225–11,230.

DeLisi, M. P., A. M. Cope, and J. K. Franklin (2001), Weekly precipitation cycles along the Northeast Corridor?, *Weather and Forecasting*, 16, 343–353.

Dessens, J., R. Fraile, V. Pont, and J. L. Sanchez (2001), Day-of-the-week variability of hail in southwestern France, *Atmos. Res.*, 59, 63–76.

Diem, J. E. (2000), Comparisons of weekday-weekend ozone: importance of biogenic volatile organic compound emissions in the semi-arid southwest USA, *Atmos. Environ.*, 34, 3445–3451.

Dusek, U., et al. (2006), Size matters more than chemistry for cloud-nucleating ability of aerosol particles, *Science*, 312(5778), 1375–1378, doi:10.1126/science.1125261.

Dye, T. S., C. P. MacDonald, C. B. Anderson, H. R. Hafner, N. J. M. Wheeler, and A. C. Chan (2003), Guidelines for Developing an Air Quality (Ozone and PM2. 5) Forecasting Program, *Tech. Rep. EPA-456/R-03-002*, U. S. Environmental Protection Agency, http://airnow.gov/index.cfm?action=static.publications.

Fujibe, F. (1987), Weekday-weekend differences of urban climates. Part 1: Temporal variation of air-temperature and other meteorological parameters in the central part of Tokyo, *J. Meteorol. Soc. Jpn.*, 65(6), 923–929.

GHCN (2007), The Global Historical Climatology Network, http://www.ncdc.noaa.gov/oa/climate/research/ghcn/ghcn.html.

Gong, D.-Y., D. Guo, and C.-H. Ho (2006), Weekend effect in diurnal temperature range in China: Opposite signals between winter and summer, *J. Geophys. Res.*, 111, D18113, doi:10.1029/2006JD007068.

Gordon, A. H. (2004), Weekdays warmer than weekends?, *Nature*, 367, 64611994.

Groisman, P. Y., R. W. Knight, T. R. Karl, D. R. Easterling, B. Sun, and J. H. Lawrimore (2004), Contemporary changes of the hydrological cycle over the contiguous United States: Trends derived from in situ observations, *J. Hydrometeor.*, 5, 64–85.

Harley, R. A., L. C. Marr, J. K. Lehner, and S. N. Giddings (2005), Changes in motor vehicle emissions on diurnal to decadal time scales and effects on atmospheric composition, *Environ. Sci. Technol.*, doi:10.1021/es048172+.

Huffman, G. J., R. F. Adler, D. T. Bolvin, G. Gu, E. J. Nelkin, K. P. Bowman, Y. Hong, E. F. Stocker, and D. B. Wolff (2007), The TRMM Multi-satellite Precipitation Analysis (TMPA): Quasi-global, multiyear, combined-sensor precipitation estimates at fine scales, *J. Hydrometeor.*, 8(1), 38–55.

Jacobson, M. Z., and Y. J. Kaufman (2006), Wind reduction by aerosol particles, *Geophys. Res. Lett.*, 33, L24814, doi:10.1029/2006GL027838.

Janowiak, J. E., V. J. Dagostaro, V. E. Kousky, and R. J. Joyce (2007), An examination of precipitation in observations and model forecasts during NAME with emphasis on the diurnal cycle, *J. Clim.*, 20(9), 1680–1692.

Jin, M., J. M. Shepherd, and M. D. King (2005), Urban aerosols and their variations with clouds and rainfall: A case study for New York and Houston, *J. Geophys. Res.*, 110(D10), D10S20, doi:10.1029/2004JD005081.

Kalnay, E., et al. (1996), The NCEP/NCAR 40-year reanalysis project, *Bull. Am. Meteorol. Soc.*, 77(3), 437–471.

Kanamitsu, M., W. Ebisuzaki, J. Woollen, S.-K. Yang, J. J. Hnilo, M. Fiorino, and G. L. Potter (2002), NCEP-DOE AMIP-II reanalysis (R-2), *Bull. Am. Meteorol. Soc.*, 83, 1632–1643, doi:10.1175/BAMS-83-11-1631.

Khain, A., D. Rosenfeld, and A. Pokrovsky (2005), Aerosol impact on the dynamics and microphysics of convective clouds, *Q. J. R. Meteorol. Soc.*, 131, 2639–2663, doi:10.1256/qj.04.62.

Koren, I., Y. J. Kaufman, L. A. Remer, and J. V. Martins (2004), Measurement of the effect of Amazon smoke on inhibition of cloud formation, *Science*, 303(5662), 1342–1345, doi:10.1126/science.1089424.

Koren, I., Y. J. Kaufman, D. Rosenfeld, L. A. Remer, and Y. Rudich (2005), Aerosol invigoration and restructuring of Atlantic convective clouds, *Geophys. Res. Lett.*, 32, L14828, doi:10.1029/2005GL023187.

Kummerow, C., et al. (2000), The status of the Tropical Rainfall Measuring Mission (TRMM) after two years in orbit, *J. Appl. Meteorol.*, 39, 1965–1982.

Kummerow, C., et al. (2001), The evolution of the Goddard Profiling Algorithm (GPROF) for rainfall estimation from passive microwave sensors, *J. Appl. Meteorol.*, 40, 1801–1820.

Langmuir, I. (1953), Final Report - Project Cirrus 53-827: Part II: Analysis of the effects of periodic seeding of the atmosphere with silver iodide, *Tech. Rep. RL-785*, General Electric Research Laboratory, Schenectady, NY.

Lawrence, E. N. (1971), Urban climate and day of the week, *Atmos. Environ.*, 5, 935–948.

Lefohn, A. S., J. D. Husar, and R. B. Husar (1999), Estimating historical anthropogenic global sulfur emission patterns for the period 1850–1990, *Atmos. Environ.*, 33, 3435–3444.

Lin, J. C., T. Matsui, R. A. Pielke Sr., and C. Kummerow (2006), Effects of biomass-burning-derived aerosols on precipitation and clouds in the Amazon Basin: A satellite-based empirical study, *J. Geophys. Res.*, 111, D19204, doi:10.1029/2005JD006884.

Lynn, B. H., A. P. Khain, J. Dudhia, D. Rosenfeld, A. Pokrovsky, and A. Seifert (2005), Spectral (bin) microphysics coupled with a mesoscale model (MM5). Part II: Simulation of a CaPE rain event with a squall line, *Mon. Weather Rev.*, 133, 59–71.

Marr, L. C., and R. A. Harley (2002), Modeling the effect of weekday-weekend differences in motor vehicle emissions on photochemical air pollution in central California, *Environ. Sci. Technol.*, 36, 4099–4106.

Mullayarov, V. A., R. R. Karimov, V. I. Kozlov, and I. N. Poddelsky (2005), Possible weekly variations in the thunderstorm activity, *J. Atmos. Sol. Terr. Phys.*, 67(4), 397–403.

Myhre, G., et al. (2006), Aerosol-cloud interaction inferred from MODIS satellite data and global aerosol models, *Atmos. Chem. Phys. Discuss.*, 6, 9351–9388.

Negri, A. J., T. L. Bell, and L. Xu (2002), Sampling of the diurnal cycle of precipitation using TRMM, *J. Atmos. Oceanic Technol.*, 19, 1333–1344.

Novakov, T., V. Ramanathan, J. E. Hansen, T. W. Kirchstetter, M. Sato, J. E. Sinton, and J. A. Sathaye (2003), Large historical changes of fossil-fuel black carbon aerosols, *Geophys. Res. Lett.*, 30(6), 1324, doi:10.1029/2002GL016345.

Olson, W. S., et al. (2006), Precipitation and latent heating distributions from satellite passive microwave radiometry. Part I: Improved method and uncertainties, *J. Appl. Meteorol. Climat.*, 45(5), 702–720.

Peixoto, J. P., and A. H. Oort (1992), *Physics of Climate*, Amer. Inst. Physics.

Perry, J. L., and P. M. Owens (2001), Weekday/weekend variability and long-term trends in traffic, CO, NOy, and ozone for the Charlotte Metropolitan Area during the 1990's, in *Proc. Air Waste Mgmt. Assoc. 94th Ann. Conf.*, available online at http://chem.winthrop.edu/faculty/owens/link_to_webpages/personal/research/CLTOzone.DOC.

Petersen, W. A., and S. A. Rutledge (2001), Regional variability in tropical convection: Observations from TRMM, *J. Clim.*, 14, 3566–3586.

Phillips, V. T. J., T. W. Choularton, A. M. Blyth, and J. Latham (2002), The influence of aerosol concentrations on the glaciation and precipitation of a cumulus cloud, *Q. J. R. Meteorol. Soc.*, 128(581), 951–971, doi:10.1256/0035900021643601.

Ramanathan, V., P. J. Crutzen, J. T. Kiehl, and D. Rosenfeld (2001), Aerosols, climate and the hydrological cycle, *Science*, 294(5549), 2119–2124, doi:10.1126/science.1064034.

Remer, L. A., et al. (2005), The MODIS aerosol algorithm, products and validation, *J. Atmos. Sci.*, 62, 947–973.

Roads, J., M. Kanamitsu, and R. Stewart (2002), CSE water and energy budgets in the NCEP-DOE Reanalysis II, *J. Hydrometeor.*, 3, 227–248.

Rosenfeld, D. (1999), TRMM observed first direct evidence of smoke from forest fires inhibiting rainfall, *Geophys. Res. Lett.*, 26(20), 3105–3108.

Rosenfeld, D. (2000), Suppression of rain and snow by urban and industrial air pollution, *Science*, 287, 1793–1796.

Rosenfeld, D. (2006), Aerosol-cloud interactions control of Earth radiation and latent heat release budgets, *Space Sci. Rev.*, *125*, 149–157, doi:10.1007/s11214-006-9053-6.

Rosenfeld, D., and C. W. Ulbrich (2003), Cloud microphysical properties, processes, and rainfall estimation opportunities, in *Radar and Atmospheric Science: A Collection of Essays in Honor of David Atlas, Meteorological Monographs*, vol. 52, edited by R. M. Wakimoto and R. Srivastava, chap. 10, pp. 237–258, Amer. Met. Soc.

Rosenfeld, D., R. Lahav, A. P. Khain, and M. Pinsky (2002), The role of sea-spray in cleansing air pollution over ocean via cloud processes, *Science*, *297*, 1667–1670.

Rudich, Y., A. Sagi, and D. Rosenfeld (2003), Influence of the Kuwait oil fires plume [1991] on the microphysical development of clouds, *J. Geophys. Res.*, *108*(D15), 4478, doi:10.1029/2003JD003472.

Salcedo, R. L. R., M. C. M. Alvim Ferraz, C. A. Alves, and F. G. Martins (1999), Time-series analysis of air pollution data, *Atmos. Environ.*, *33*, 2361–2372.

Seifert, A., and K. D. Beheng (2005), A two-moment cloud microphysics parameterization for mixed-phase clouds. Part 2: Maritime vs. continental deep convective storms, *Meteorol. Atmos. Phys*, doi:10.1007/s00703-005-0113-3.

Shutters, S., and R. C. Balling Jr. (2006), Weekly periodicity of environmental variables in Phoenix, Arizona, *Atmos. Environ.*, *40*, 304–310.

Simmonds, I., and J. Kaval (1986), Day-of-the-week variation of rainfall and maximum temperature in Melbourne, Australia, *Archs. Meteorol. Geophys. Bioclimatol.*, *B36*, 317–330.

Simmonds, I., and K. Keay (1997), Weekly cycle of meteorological variations in Melbourne and the role of pollution and anthropogenic heat release, *Atmos. Environ.*, *31*(11), 1589–1603.

Teller, A., and Z. Levin (2006), The effects of aerosols on precipitation and dimensions of subtropical clouds: a sensitivity study using a numerical cloud model, *Atmos. Chem. Phys.*, *6*, 67–80.

TRMM PR Team (2005), Tropical Rainfall Measuring Mission (TRMM) Precipitation Radar Algorithm Instruction Manual for Version 6, NASDA/NASA, available online at http://www.eorc.jaxa.jp/TRMM/document/pr_manual/pr_manual_v6.pdf.

USEPA (2006), Air Quality System, Office of Air Quality Planning and Standards, U. S. Environmental Protection Agency, http://www.epa.gov/ttn/airs/airsaqs/.

van den Heever, S. C., G. G. Carrió, W. R. Cotton, P. J. Demott, and A. J. Prenni (2006), Impacts of nucleating aerosol on Florida storms. Part I: Mesoscale simulations, *J. Atmos. Sci.*, *63*(7), 1752–1775.

Vose, R. S., R. L. Schmoyer, P. M. Steurer, T. C. Peterson, R. Heim, T. R. Karl, and J. Eischeid (1992), The Global Historical Climatology Network: Long-term monthly temperature, precipitation, sea level pressure, and station pressure data, *Tech. Rep. ORNL/CDIAC-53, NDP-041*, Carbon Dioxide Information Analysis Center, Oak Ridge National Laboratory, Oak Ridge, Tennesse.

Wåhlin, P., F. Palmgren, and R. V. Dingenen (2001), Experimental studies of ultrafine particles in streets and the relationship to traffic, *Atmos. Environ.*, *35*, S63–S69.

Wang, C. (2005), A modeling study of the response of tropical deep convection to the increase of cloud condensation nuclei concentration: 1. Dynamics and microphysics, *J. Geophys. Res.*, *110*, D21211, doi:10.1029/2004JD005720.

Wild, M., et al. (2005), From dimming to brightening: Decadal changes in solar radiation at Earth's surface, *Science*, *308*(5723), 847–850, doi:10.1126/science.1103215.

Wilks, D. S. (1997), Resampling hypothesis tests for autocorrelated fields, *J. Clim.*, *10*(1), 65–82.

Williams, E., et al. (2002), Contrasting convective regimes over the Amazon: Implications for cloud electrification, *J. Geophys. Res.*, *107*(D20), 8082, doi:10.1029/2001JD000380.

Wilson, W. E. (2002), Monitoring of particulate matter outdoors, *Chemosphere*, *49*(9), 1009–1043.

Zipser, E. J., and K. R. Lutz (1994), The vertical profile of radar reflectivity of convective cells: A strong indicator of storm intensity and lightning probability?, *Mon. Weather Rev.*, *122*, 1751–1759.

———————————

T. L. Bell, K.-M. Kim, and M.-I. Lee, NASA/Goddard Space Flight Center, Mail Code 613.2, Greenbelt, MD 20771, USA. (thomas.l.bell@nasa.gov; kyu-myong.kim@nasa.gov; myong-in.lee@nasa.gov)

M. Hahnenberger, Meteorology Department, University of Utah, Salt Lake City, UT 84112-0110, USA. (mhahn@met.utah.edu)

D. Rosenfeld, Institute of Earth Sciences, The Hebrew University of Jerusalem, 91904 Givat Ram, Jerusalem, Israel. (daniel@vms.huji.ac.il)

J.-M. Yoo, Department of Science Education, Ewha Womans University, 11-1, Daehyun-Dong, Seodaemun-Gu, Seoul, South Korea 120-750. (yjm@ewha.ac.kr)